Research Paper

GEOSPHERE

GEOSPHERE, v. 18, no. 4

https://doi.org/10.1130/GES02447.1

12 figures; 3 tables

CORRESPONDENCE: wcraddock@usgs.gov

CITATION: Craddock, W.H., O'Sullivan, P.B., and McAleer, R.J., 2022, U-Pb and fission-track data from zircon and apatite resolve latest- and post-Alleghanian thermal histories along the Fall Line of the Atlantic margin of the southeastern United States: Geosphere, v. 18, no. 4, p. 1330–1353, https://doi.org/10.1130/GES02447.1.

Science Editor: David E. Fastovsky
Associate Editor: G. Lang Farmer

Received 4 May 2021
Revision received 19 November 2021
Accepted 16 March 2022

Published online 10 June 2022

U-Pb and fission-track data from zircon and apatite resolve latest- and post-Alleghanian thermal histories along the Fall Line of the Atlantic margin of the southeastern United States

William H. Craddock[1], Paul B. O'Sullivan[2], and Ryan J. McAleer[3]

[1]Geology, Energy, and Minerals Science Center, U.S. Geological Survey, Reston, Virginia 20192, USA
[2]GeoSep Services, Inc., Moscow, Idaho 83843, USA
[3]Florence Bascom Geoscience Center, U.S. Geological Survey, Reston, Virginia 20192, USA

ABSTRACT

Although the Atlantic continental margin of the eastern United States is an archetypal passive margin, episodes of rejuvenation following continental breakup are increasingly well documented. To better constrain this history of rejuvenation along the southern portion of this continental margin, we present zircon U-Pb (ZUPb) age, zircon fission-track (ZFT) age, apatite U-Pb (AUPb) age, and apatite fission-track (AFT) age and length data from six bedrock samples. The samples were collected along the boundary between the exposed Appalachian hinterland (Piedmont province) and the updip limit of passive margin strata (Coastal Plain province). The samples were collected from central Virginia southward to the South Carolina–Georgia border. ZUPb age distributions are generally consistent with geologic mapping in each of the sample areas. The AUPb data are highly discordant owing to high common-Pb abundances, but for two plutons at the northern and southern ends of the sample area, they define a discordia regression line that indicates substantial Permo-Triassic exhumation-driven cooling. ZFT age distributions are highly dispersed but define central values ranging from Permian to Jurassic. AFT data mostly appear to define a singular underlying cooling age, generally approximately Jurassic or Early Cretaceous. Apatite fission tracks are moderately long (mean lengths in the range of ~13.5 µm), however track lengths for one sample in central North Carolina are shorter (~12.5 µm). To interpret the post-breakup thermal history, we present inverse models of time-temperature history for the five plutonic samples. The models show a history of (1) rapid cooling (>10 °C/m.y.) from deep-crustal to near-surface temperatures by the Triassic, (2) hundreds of degrees of Triassic reheating, (3) Jurassic–Early Cretaceous cooling (at rates of 1–10 °C/m.y.), and (4) slow Late Cretaceous–Cenozoic cooling (~1 °C/m.y.). An additional suite of forward models is presented to further evaluate the magnitude of maximum Triassic reheating at one sample site that is particularly well constrained by thermal maturity data. The model results and geologic reasoning suggest that the inverse models may overestimate Triassic paleotemperatures but that other aspects of the inverse modeling are robust. Overall, this thermal history can be reconciled with several aspects of the lithostratigraphy of distal parts of the continental margin, including the lack of Jurassic–earliest Cretaceous strata beneath the southern Atlantic coastal plain and Cretaceous–Cenozoic grain-size trends.

William Craddock https://orcid.org/0000-0002-4181-4735

INTRODUCTION

Rifting of supercontinent Pangea is archived in the southeastern United States by an elongate chain of approximately Late Triassic extensional basins that extends parallel to the continental margin (e.g., Olsen, 1997; Withjack et al., 1998). The timing of subsequent continental breakup is bracketed by the age of the oldest oceanic crust adjacent to this continental margin, which is thought to be ca. 175 Ma (Withjack et al., 1998; Müller et al., 2008). Around the southeastern Atlantic margin, the rift basins show structural evidence for inversion (see Withjack et al., 1998, and references therein). Moreover, Triassic basins exposed in the Appalachian Piedmont province and those beneath updip portions of the coastal plain exhibit elevated near-surface thermal maturity that implies kilometer-scale exhumation of these basins (e.g., Reid and Milici, 2008; Malinconico, 2015). Beneath offshore areas, the sag phase of basin fill appears to be absent in seismic reflection data likely due to erosion (Post et al., 2016).

For the area from the state of Virginia to the south, few studies have focused on the timing of the inversion of the rift-basin province. Thermochronological studies of the southern Appalachian orogen indicate kilometer-scale exhumational cooling since the Cretaceous (e.g., Roden, 1991; Roden et al., 1993; Boettcher and Milliken, 1994; Spotila et al., 2004; McKeon et al., 2014). However, most of these studies have been focused to the west of the rift basins in the western portions of the Piedmont province, the Blue Ridge province, or the Appalachian orogenic foreland basin (Fig. 1). The sedimentary record offshore of Maryland and Virginia records accelerations in sediment supply in the Jurassic, in the Hauterivian–Barremian, in the Campanian, and in the Neogene owing to changes in erosion upstream (Poag and Sevon, 1989; Pazzaglia and Brandon, 1996), but a similar analysis for more southerly parts of the continental margin and source-sink studies remains outstanding.

This paper presents the results of a study on the post-Paleozoic thermal and erosional history of the

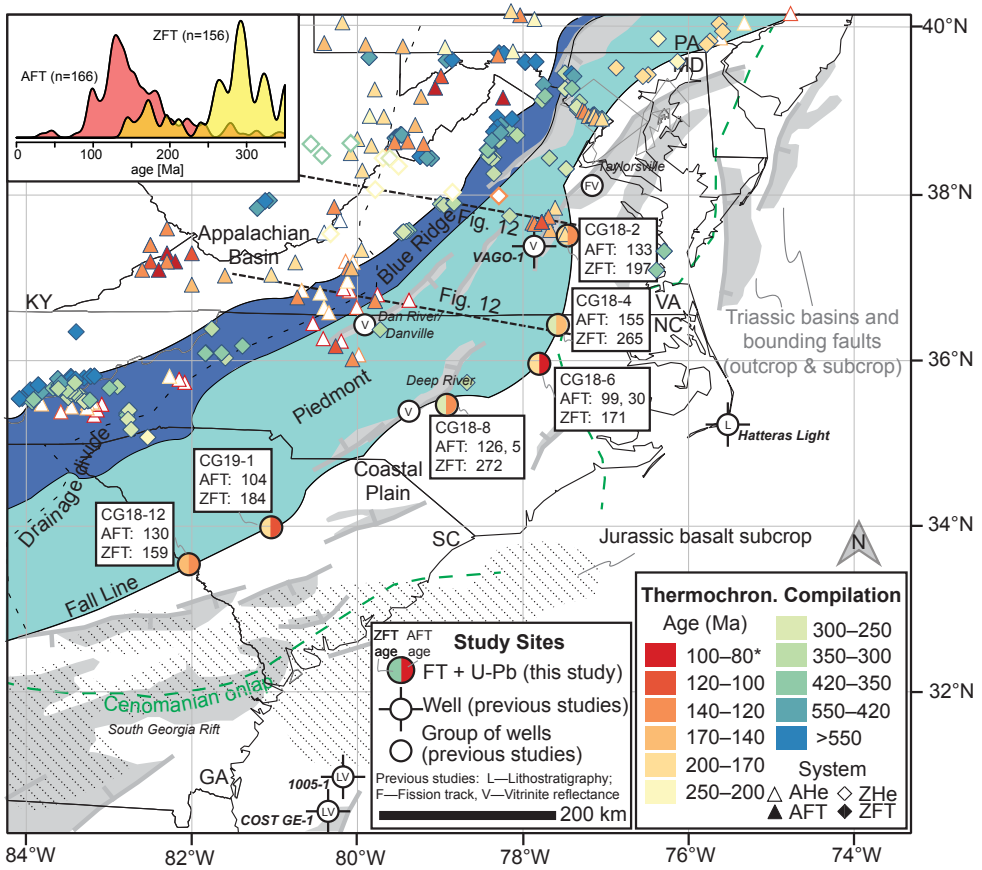

Figure 1. Apatite fission-track (AFT), zircon fission-track (ZFT), apatite (U-Th)/He (AHe), and zircon (U-Th)/He (ZHe) samples across the southern Appalachians (eastern United States), including the six new AFT-ZFT samples presented in this paper. At the six new sites, apatite and zircon U-Pb geo- and thermochronologic data were also collected and are presented in this paper. For AFT samples, central ages are given, with all age modes given for multimodal AFT age distributions. For ZFT samples, filtered central ages are presented. Inset plot shows a kernel density function for all previously published AFT and ZFT samples. Previously published AFT-ZFT data are from Durrant (1979), Roden and Miller (1989), Roden (1991), Kohn et al. (1993), Roden et al. (1993), Blackmer et al. (1994), Boettcher and Milliken (1994), Spotila et al. (2004), Kunk et al. (2005), and Naeser et al. (2016). AHe data are from Spotila et al. (2004) and McKeon et al. (2014). ZHe data are from Basler et al. (2021). Triassic faults and subcrop and outcrop are after Withjack et al. (1998) and Reed et al. (2005). Outline of interpreted extent of mafic magmatic rocks is from McBride et al. (1989). Updip preservation limit of Cenomanian–Turonian strata beneath the Atlantic coastal plain of the southeastern United States is after Owens and Gohn (1985). FT—fission track; Thermochron.—Thermochronology; *—three samples with ages <80 Ma are color coded this shade of red. GA—Georgia; SC—South Carolina; NC—North Carolina; VA—Virginia; MD—Maryland; PA—Pennsylvania; KY—Kentucky.

southeastern part of the continental margin, at the boundary of the exposed part of the southern Appalachian orogen and the passive-margin sequence beneath the physiographic coastal plain. This boundary is referred to as the "Fall Line," named for the bedrock river knickzones that are located along the strike of this feature. The key new data are zircon fission-track (ZFT) age measurements and apatite fission-track (AFT) age and length measurements for each of six samples collected from Fall Line outcrops from central Virginia to the Georgia–South Carolina border. To constrain the long-term thermal history of these samples, we also present paired zircon U-Pb (ZUPb) age measurements and, where possible, apatite U-Pb (AUPb) data as well.

A suite of inverse models of time-temperature history for the five fission-track samples from plutons is presented to help in understanding the regional post-breakup thermal history. The inverse models involve at least one major geological assumption, which is that samples were cooled to near-surface temperatures by the Triassic and subsequently reheated. An additional suite of forward models that involves a larger number of geological assumptions is presented in the Discussion section. The objective of the forward models is to constrain a geological interpretation that reconciles thermochronologic constraints on Triassic heating with constraints from vitrinite reflectance (VR) data from Triassic extensional basins around the region (e.g., Reid and Milici, 2008; Malinconico, 2015). We compare our interpretations of thermal and geological history with preservation limits of passive-margin strata. We also compare these data to previously published AFT and ZFT data from around the southern Appalachian orogen as well as the lithostratigraphic character of more distal Jurassic–Cenozoic stratigraphic sections known from wells.

BACKGROUND

Age and Thermal Maturity of Extensional Basin Fill

In the southern portion of the Appalachian orogen (herein, the portion of the orogen extending

from Virginia to the south), the easternmost exposed rocks are igneous and metamorphic rocks of the Appalachian Piedmont province (Fig. 1). The province consists of deeply eroded rocks that were accreted onto the margin of the North American craton during the Paleozoic and represent part of the composite Paleozoic orogenic hinterland (e.g., Hatcher, 1987). Triassic extensional basins are inset into these rocks (e.g., Olsen, 1997). These same deeply eroded hinterland rocks inset with Triassic extensional basins extend eastward toward the continental margin, however they are covered by a younger Mesozoic–Cenozoic passive-margin sequence to the east. The updip limit of the passive-margin strata is the Fall Line.

The age of the basin fill within the Triassic extensional basins is well studied, at least where basins crop out or have been cored (e.g., Olsen, 1997, and references therein). The age of the oldest strata preserved in these basins is ca. 230 Ma. The youngest preserved strata generally range in age from 225 to 215 Ma, however the South Georgia Rift basin contains strata as young as ca. 200 Ma. VR measurements in Taylorsville, Richmond, Deep River, and Dan River Basins all indicate elevated near-surface thermal maturity in these basins (Fig. 1; Reid and Milici, 2008; Malinconico, 2015). Moreover, previous workers have reported reset AFT and ZFT measurements and fluid inclusion–based analysis of maximum paleotemperatures from basal strata in the Taylorsville Basin (Roden and Miller, 1991; Tseng et al., 1996), all of which are consistent with ~100 °C of cooling from maximum paleotemperatures. This cooling event has generally been attributed to kilometer-scale exhumation (e.g., Tseng et al., 1996).

Mesozoic Volcanism

In the subsurface area around the South Georgia Rift basin, flood basalt and diabase separate deformed Triassic strata from overlying, flat-lying passive-margin strata (Fig. 1; McBride et al., 1989). A regionally extensive seismic reflector has been interpreted to record the extent of this basalt (McBride et al., 1989). Well data verify the presence of the basalt in some locations, although the degree to which the reflector exclusively indicates the presence of magmatic rocks has been called into question (Heffner et al., 2012). A range of whole-rock $^{40}Ar/^{39}Ar$ plateau and total-fusion ages (236–161 Ma) was reported for these basalts, with a ca. 183 Ma plateau age appearing to be the most reflective of the timing of crystallization (Lanphere, 1983). However, some workers correlate the basalts to a ca. 200 Ma dike swarm that extends from the South Carolina Piedmont to the north and to the larger ca. 200 Ma Central Atlantic magmatic province based on the geologic context of the samples (Hames et al., 2000; Olsen et al., 2003; Heffner et al., 2012). Subsequent phases of intraplate volcanism in approximately the Late Jurassic and Eocene are also recorded in the map area, but these episodes were confined to the northwestern part of the map area in the Appalachian foreland province (e.g., Mazza et al., 2017).

Post-Rift Stratal Packages

Beneath much of the Atlantic coastal plain of the southeastern United States, the oldest preserved passive-margin strata date to the middle part of the Cretaceous, from about Aptian–Albian to about Coniacian–Santonian depending on the location (Fig. 1; Owens and Gohn, 1985). Age control for these basal passive-margin strata is commonly difficult to obtain owing to the fact that they are coarse grained, nonmarine, lacking in diagnostic fossil assemblages, and also lacking in volcanic ash or other material amenable to radiometric dating (Scholle, 1979). However, older, Tithonian strata are thought to be preserved beneath the downdip areas of Cape Hatteras, North Carolina (Brown et al., 1972; Almy, 1987) and southern Florida (Applegate et al., 1981) and more widely offshore (Dillon and Popenoe, 1988). There are limited well penetrations of downdip stratigraphic sections, but two of the more distal (groupings of) deep wells are in the Cape Hatteras area of North Carolina as well as the area offshore of Georgia (Fig. 1; Table 1).

Thermochronological Records of Post-Paleozoic Erosion

The ZFT, AFT, and apatite (U-Th)/He (AHe) thermochronometers have been widely applied to understanding the Mesozoic erosion of the southern Appalachian orogen (Fig. 1). Effective closure temperatures (at cooling rates of 10 °C/m.y.) for the ZFT system have been reported as anywhere from 342 to 232 °C (Reiners and Brandon, 2006). Higher closure-temperature estimates have generally been obtained for zircon grains lacking radiation damage, and the wide range is likely a function of the degree of radiation damage (Rahn et al., 2004; Ketcham, 2016). The AFT thermochronometer has a closure temperature of ~116 °C (for apatite with average composition; Reiners and Brandon, 2006). The AHe

TABLE 1. WELL INFORMATION

Name and no.	API	Latitude (°N)	Longitude (°W)	Total depth (m)	Datum elevation (m)	Datum*	Operator
COST GE-1	61-184-00001	30.61889	80.29972	4040	30	KB	Ocean Production
Brunswick 1005-1	61-185-00002	30.99278	80.24389	3546	31	KB	Transco
Hatteras Light 1	32-055-00001	35.25168	75.52912	3064	7	GL	Standard Oil
VAGO-1	n/a	37.60333	77.69111	48	77	GL	Phillips Coal Company

*KB—kelly bushing, GL—ground level.
Note: API column contains American Petroleum Institute numbers that uniquely identify United States oil and gas wells. n/a—not applicable. Well locations shown in Figure 1.

thermochronometer has a closure temperature of ~67 °C at cooling rates of 10 °C/m.y. (Reiners and Brandon, 2006, and references therein). Recent work has pioneered the use of the zircon (U-Th)/He (ZHe) system in the southern part of the Appalachian orogen (Basler et al., 2021). At the cooling rates cited above, the system has a closure temperature of 183 °C (Reiners and Brandon, 2006), such that it constrains a temperature window that is between those of the ZFT and AFT systems.

Zircon fission-track ages exhibit a west-to-east gradient across the Appalachian orogen (Fig. 1). In the foreland of the orogen, ZFT ages are generally Precambrian, are generally older than the depositional ages of the rock, and therefore are generally unreset (Naeser et al., 2016). In the Blue Ridge province, the ages are generally Paleozoic and record in situ cooling histories. The few reported ZFT ages in the western Piedmont province appear to record exhumation during the Alleghanian orogeny in the Carboniferous–Permian (Kunk et al., 2005; Naeser et al., 2016). However, farther to the northeast, post-Alleghanian, Triassic–earliest Jurassic ZFT ages are reported, both in pre-Mesozoic rocks of northeastern Maryland and southeastern Pennsylvania and in Triassic strata of Taylorsville Basin in northeastern Virginia (Roden and Miller, 1991). The young ages to the north (Maryland and Pennsylvania) are inferred to reflect a thermal overprint owing to magmatic heating at ca. 200 Ma (northeasternmost samples on Fig. 1; Kohn et al., 1993), whereas the Triassic stratal samples were interpreted to record in situ exhumational cooling in the Taylorsville Basin (e.g., Roden and Miller, 1991; Tseng et al., 1996).

Similarly to ZFT ages, ZHe ages exhibit a west-to-east gradient across the orogen at the latitude of central Virginia (Basler et al., 2021). Whereas the system is unreset in the distal, undeformed part of the foreland, it provides a thermochronological record of Pennsylvanian–Permian exhumational cooling in the proximal foreland and in the Blue Ridge province (Basler et al., 2021). Farther still to the east, in the Piedmont province, the ZHe system records in situ cooling in the Jurassic–Early Cretaceous (Basler et al., 2021).

Patterns in AFT ages show that post-Paleozoic erosion of the Appalachians has been more extensive in the interior portions of the orogen, at least since the Cretaceous. AFT samples from the west of the modern continental divide (in the Appalachian foreland basin) are characterized by a mix of Jurassic and Cretaceous cooling ages (e.g., Roden, 1991; Roden et al., 1993; Boettcher and Milliken, 1994; see also Roden and Miller [1989] and Blackmer et al. [1994] for the area to the north in Pennsylvania). In combination with the Paleozoic ZHe ages across a similar area, the AFT data imply a long period of erosional quiescence in the foreland from the end of the Paleozoic to the Jurassic or Cretaceous (e.g., Basler et al., 2021). To the east of the continental divide, AFT ages in the Blue Ridge and Piedmont provinces (and in the northeasterly portion of the foreland in this study area) are not as widely reported and are more uniformly Cretaceous (e.g., Spotila et al., 2004).

The spatial distribution of published AHe ages is more restricted than that of ages derived from the fission-track thermochronometers. Data from the highest-elevation parts of the Blue Ridge in southwestern North Carolina, near the modern continental divide, resolve a period of relief generation that occurred between ca. 120 and 60 Ma but do not resolve any periods of exceptionally rapid erosion within that time window (McKeon et al., 2014). Farther to the east in the orogen, Late Cretaceous ages in the Piedmont province of southern Virginia and northern North Carolina are generally younger than ages in adjacent parts of the Blue Ridge uplands, a pattern which has been interpreted in the context of Cretaceous–Cenozoic westward retreat of the Blue Ridge province topographic escarpment, which is thought to have formed at the time of continental rifting and breakup (Spotila et al., 2004). In general, published thermochronological data are much more sparse in the easterly portions of the Piedmont (Fig. 1).

METHODS

Compilation of Thermochronological Data

We compiled AFT and ZFT data from seven published reports covering the study area (Roden, 1991; Kohn et al., 1993; Roden et al., 1993; Boettcher and Milliken, 1994; Spotila et al., 2004; Kunk et al., 2005; Naeser et al., 2016) and two additional reports covering the northernmost edge of the map area in Figure 1 (Roden and Miller, 1989; Blackmer et al., 1994). We also include eight AFT and six ZFT ages reported in an unpublished master's thesis (Durrant, 1979) and cited by subsequent authors (e.g., Gates and Glover, 1989; Owens et al., 2017). Central ages are used to represent samples (e.g., Fig. 1) when those ages were provided by the original author, generally for samples that do not pass the chi-squared test of homogeneity. For all other samples, pooled ages are used. The area of subsurface AFT and ZFT sampling by Roden and Miller (1991; see also Tseng et al., 1996; see the previous study site located in Taylorsville basin) is also noted on Figure 1, although only outcrop samples are displayed on the map. Other subsurface sample locations from Appalachian basin (e.g., Blackmer et al., 1994; Reed et al., 2005) are not shown owing to the high density of outcrop sample coverage in the foreland. AHe data were compiled from two additional reports and represent either average ages (Spotila et al., 2004) or pooled ages (McKeon et al., 2014), based on the reporting by the original authors. The locations of ZHe samples reported by Basler et al. (2021) are also shown on Figure 1. Samples are color-coded according to the age of the youngest replicate. Readers are directed to these original studies for additional summaries of the data.

Sampling

Six bedrock samples were collected for ZUPb, AUPb, ZFT, and AFT analysis at field sites with bedrock exposure where large rivers cross the Fall Line, from the James River in Virginia to the Savannah River on the border of South Carolina and Georgia (Figs. 1, 2; Table 2). Five of the samples are from plutonic rocks and one is from metasedimentary rocks. The sampling strategy was guided partly by the fact that bedrock samples were collected alongside modern river-sediment samples for paired detrital thermochronologic analysis. The samples for this study were collected in situ from around the

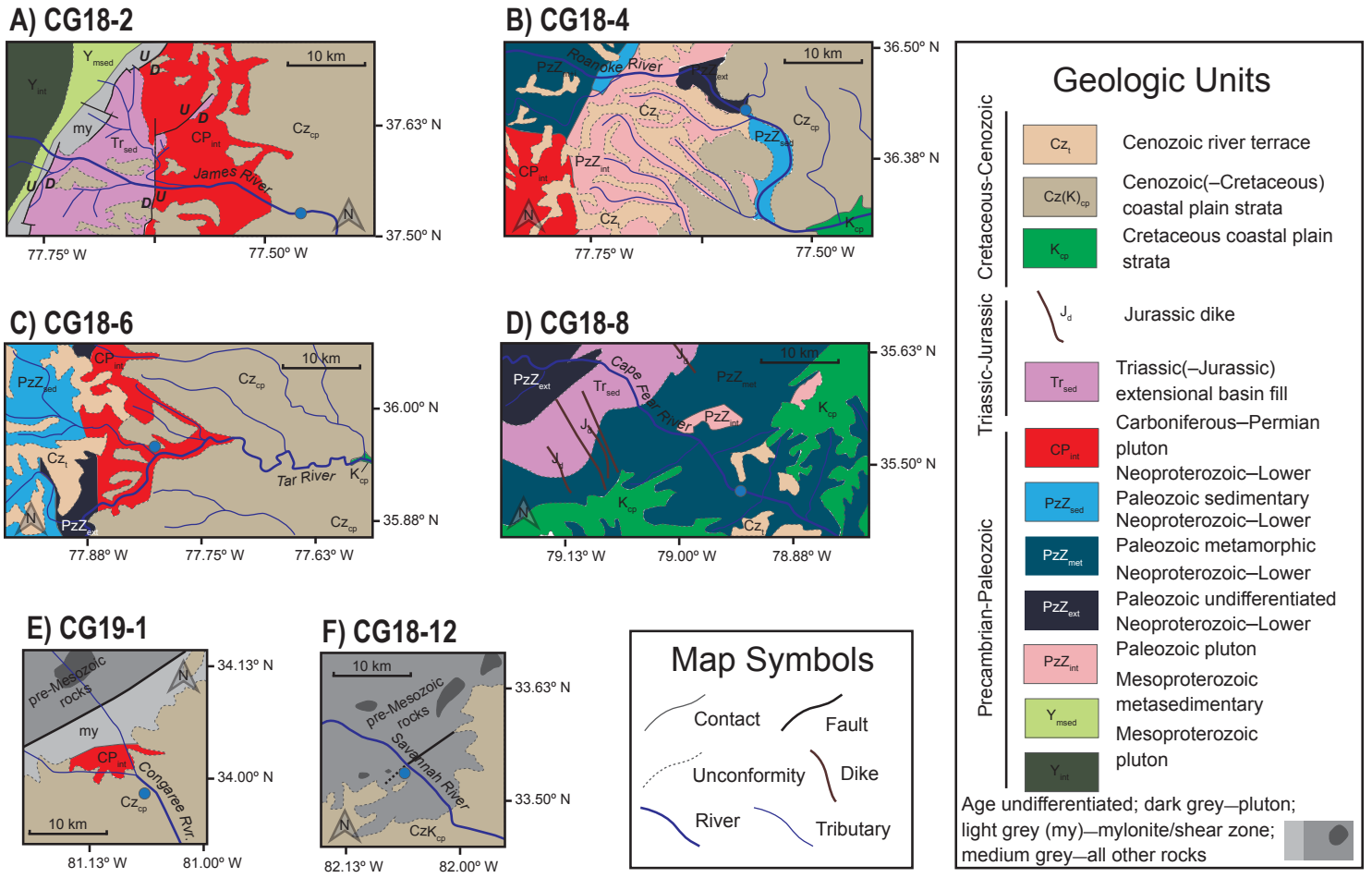

Figure 2. Geologic maps of sample sites (blue circles). (A) Map for sample CG18-2, Pennsylvanian–Permian Petersburg Granite, collected along the James River in Richmond, Virginia. In this panel, faults are extensional, with "D" and "U" marking the downthrown and upthrown blocks, respectively. (B) Map for sample CG18-4, Neoproterozoic metamorphosed tonalite, collected along the Roanoke River in Weldon, North Carolina. (C) Map for sample CG18-6, Pennsylvanian–Permian granite collected along the Tar River in Rocky Mount, North Carolina. (D) Map for sample CG18-8, Neoproterozoic–Paleozoic schist collected along the Cape Fear River east of Sanford, North Carolina. (E) Map for sample CG19-1, Pennsylvanian–Permian Columbia Granite, collected near the Congaree River in Columbia, South Carolina. (F) Map for sample CG18-12, Paleozoic metagranite, collected along the Savannah River in Augusta, Georgia. Geologic mapping in A is from Marr (2002); geologic mapping in B, C, and D is from North Carolina Geological Survey (1985); geologic mapping in E is from Horton and Dicken (2001); and geologic mapping in F is from Horton and Dicken (2001) (northeast of river) and Lawton et al. (1976) (southeast of river).

TABLE 2. SAMPLE INFORMATION

Field ID	River	Latitude (°N)	Longitude (°W)	Elevation (m)	Rock unit	Rock type	Age
CG18-2	James	37.5258	77.4568	13	Petersburg Granite	Metamorphosed granite	Pennsylvanian–Permian
CG18-4	Roanoke	36.4273	77.5915	11	Roanoke Rapids terrane	Weakly metamorphosed tonalite	Neoproterozoic
CG18-6	Tar	35.9612	77.8039	21	Unnamed	Weakly metamorphosed granite	Permian
CG18-8	Cape Fear	35.4791	78.9307	39	Unnamed	Schist	Ordovician–Neoproterozoic
CG19-1	Congaree	33.9853	81.0531	80	Columbia Granite	Metamorphosed granite	Pennsylvanian–Permian
CG18-12	Savannah	33.5481	82.0359	49	Unnamed	Metamorphosed granite	Ordovician(?)–Devonian(?)

outcrop and aggregated into a composite sample. This strategy was implemented to obtain apatite and zircon yields sufficiently large for fission-track analysis.

U-Pb and Fission-Track Age Determination of Apatites and Zircons

Mineral separation and geo- and thermochronologic analysis were conducted by GeoSep Services (Moscow, Idaho, USA). Zircons and apatite grains were separated from bulk-rock samples using the following steps: jaw crusher, 300 µm sieve, centrifuge in a heavy liquid (lithium polytungstate), and magnetic separator.

Measurement of fission-track cooling age and track length distributions were conducted following methods outlined in Donelick et al. (2005) and Chew and Donelick (2012). For each sample, 25 zircon or 40 apatite grains were analyzed. The grains were mounted in epoxy, polished, and etched using 5.5 M nitric acid for 20.0 s (± 0.5 s). Zircons were etched in a eutectic melt of NaOH + KOH at ~210 °C (± 10 °C) for the time necessary to adequately reveal spontaneous fission tracks intersecting the grain surfaces. Spontaneous fission tracks intersecting a measured area of the polished grain surface were counted using a petrographic microscope. Apatite mounts were then subjected to ^{252}Cf-derived fission fragment irradiation and etched again to reveal confined spontaneous fission tracks for length measurements. Fission-track lengths were not measured in zircon owing to the incompletely understood annealing kinetics. For each apatite sample, ~200 confined track lengths were measured using a petrographic microscope, as was the angle of each track to the crystallographic *c*-axis. For every apatite grain that was analyzed, maximum etch pit diameter parallel to the *c*-axis (D_{par}) was determined. For each spot over which fission tracks were counted, ^{238}U was measured as a ratio to a lighter, abundant isotope (^{43}Ca for apatite; ^{29}Si for zircon) by an Agilent 7700x quadrupole inductively coupled plasma mass spectrometer equipped with a New Wave Nd-YAG 213 nm laser ablation system at Washington State University Geoanalytical Laboratory (Pullman, Washington, USA). The lighter isotopes provide some indication of the volume of ablated material. A 20-µm-diameter ablation spot was used for apatites, and a 30-µm-diameter ablation spot was used for zircons. The laser output power was set to 8 J/cm and the frequency to 5 Hz, and apatite and zircon ablation pit depths typically ranged from 16 to 18 µm and 12 to 15 µm, respectively. Measurements of ^{238}U/^{43}Ca and ^{238}U/^{29}Si were used to determine fission-track ages using a zeta-calibration approach with reference to Durango apatite and Fish Canyon tuff zircon as age standards (Hasebe et al., 2004; Donelick et al., 2005).

Determination of U-Pb ages was coeval with the fission-track mass spectrometry. Under the laser conditions described above, signal data were collected by scanning repeatedly across the following isotopic masses for apatite: ^{43}Ca, ^{147}Sm, ^{204}Pb, ^{206}Pb, ^{207}Pb, ^{232}Th, and ^{238}U. The same isotopic masses were scanned in zircon except that ^{29}Si was substituted for ^{43}Ca. Apatite from the Duluth Complex (Minnesota, USA; 1099.0 ± 0.6 Ma; Paces and Miller, 1993) and the McClure Mountain syenite (ca. 523.98 ± 0.12 Ma; Schoene and Bowring, 2006) were used as primary and secondary standards. Zircon from the Duluth Complex (1099.0 ± 0.6 Ma; Paces and Miller, 1993) and the Tardree rhyolite (ca. 61.23 ± 0.11 Ma; Ganerød et al., 2011) were used as primary and secondary standards. Five spots on each standard were analyzed at the beginning and end of each analytical session. For every ~25–30 measurements on primary/secondary standards or unknowns, an additional three measurements were made both on the FT standard and the primary U/Pb standard. The data are corrected for common Pb using the measured atomic mass of 204 amu (atomic mass units) and assuming the initial Pb concentrations from Stacey and Kramers (1975). Ages for the ratios ^{207}Pb/^{235}U$_c$, ^{206}Pb/^{238}U, and ^{207}Pb/^{206}Pb (where ^{235}U$_c$ = ^{238}U/137.88) were calculated for each data scan and checked for concordance; concordance here was defined as overlap of all three ages at the 1σ level. Data were collected during 30 laser scans. AUPb analytical methods were similar to those above and also similar to methods described by Chew and Donelick (2012).

All ZUPb, AUPb, ZFT, and AFT data are archived permanently online in machine-readable format with metadata (Craddock and O'Sullivan, 2021). All samples were examined using a petrographic microscope and all zircon slides were imaged using cathodoluminescence (CL) following the other analytical work (Figs. 3, 4).

Presentation of Analytical Data

All analytical data are presented in a U.S. Geological Survey data release that is permanently archived online (Craddock and O'Sullivan, 2021). The ZUPb isotope and age data are displayed on both Wetherill

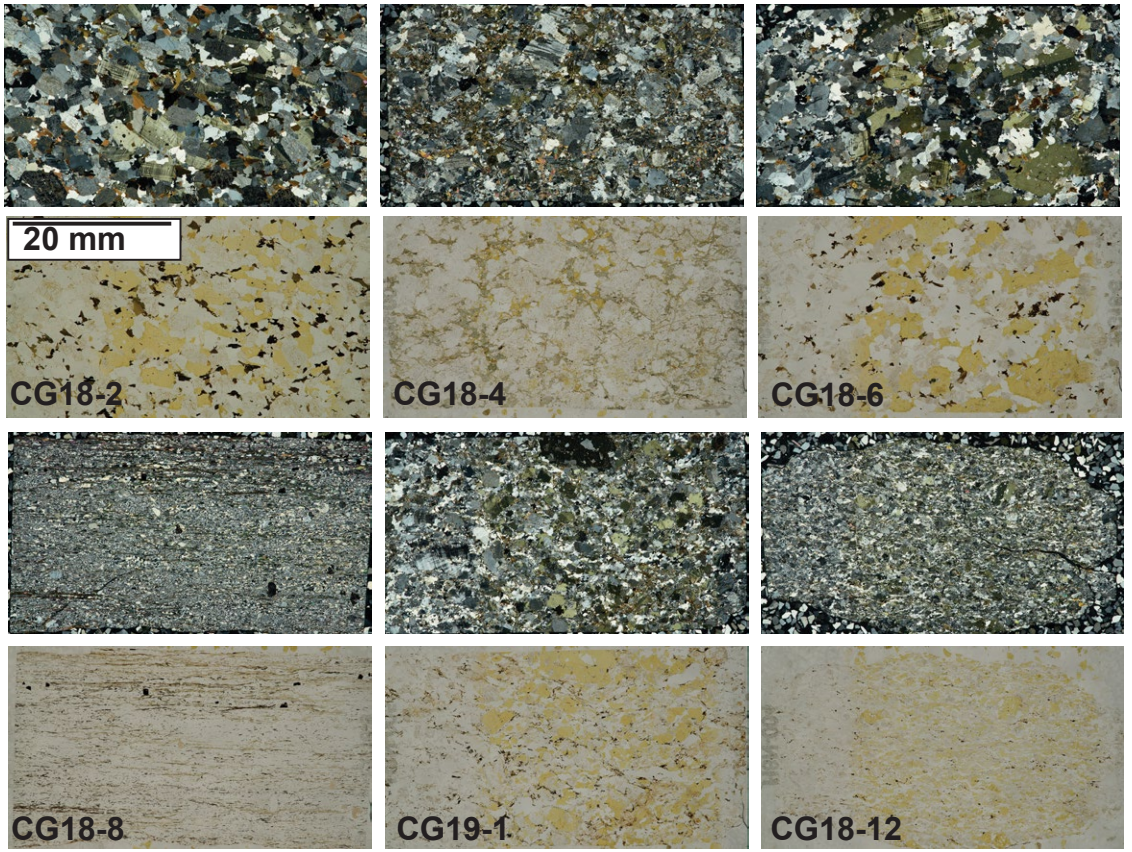

Figure 3. Petrographic images of samples. Upper image is in cross-polarized light; lower image is in plane-polarized light. Sodium colbaltinitrite staining in the right two-thirds of the field of view makes K-feldspar appear tan-yellow in plane-polarized light. Scale is the same in all images.

concordia diagrams and weighted average plots (Fig. 5; Ludwig, 2012; Vermeesch, 2018). Nearly all zircon grains yielded concordant scans (see Methods section). Because we consider the concordant scan data to be better suited for graphical comparison to ZFT measurements, we use concordant scan data on the Wetherill plots. For the metasedimentary sample, the age distribution is shown on a histogram. For igneous samples, age distributions are shown on weighted mean age plots, and the weighted mean age and uncertainty of the analyses interpreted to reflect crystallization are reported. For samples that yielded robust AUPb data (igneous samples only), isotope ratios are displayed on Tera-Wasserburg concordia diagrams (Fig. 6). Discordia regression lines generated using the IsoplotR toolbox (Vermeesch, 2018) define the cooling age and common Pb at the time of apatite crystallization (e.g., Chew and Donelick, 2012). Almost no apatite analyses yielded concordant U-Pb isotope ratios. Therefore, the overall isotope ratio is plotted for each ablation spot, and we do not present graphical comparisons of AUPb versus AFT ages. In the text, all ZUPb and AUPb age uncertainties are reported at 2σ, unless the mean square weighted deviation (MSWD) is >2.5, in which case the reported error is multiplied by the square root of the MSWD.

The ZFT data are displayed on plots that show ZFT age histograms and cross-plots of ZFT versus ZUPb age on a single display (Fig. 7). We also show comparisons of ZFT age and effective uranium ($eU = U + 0.235 \times Th$) concentration in insets within the ZFT plots (Fig. 7A). In many instances, ZFT age distributions appear to exhibit multiple age modes. Particularly for plutonic rocks, this suggests the presence of multiple annealing kinetic populations. Distinct, very young (<100 Ma) age modes are not regarded as geologically plausible in this field area and were thus filtered. Distinct clusters of older ZFT ages that overlap with, or even pre-date, the paired ZUPb age were also filtered. We report central ages for both the filtered and unfiltered age distributions. In most instances, ZFT ages correlate to eU concentration (McDannell et al., 2019) concentration. This correlation suggests that the annealing kinetics

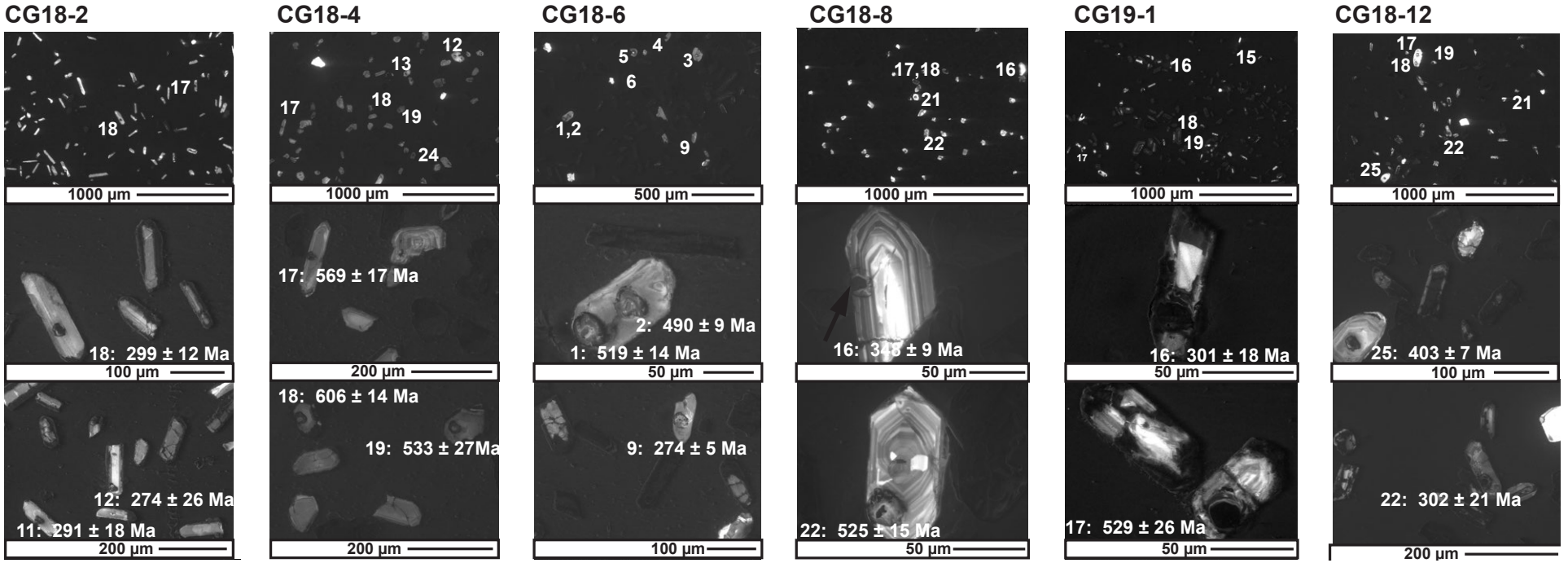

Figure 4. Cathodoluminescence images of zircon grains from different samples. Uppermost image for each sample shows a representative suite of tens of zircon grains; lower images show representative grains. Number beside each grain is the laser ablation–inductively coupled plasma–mass spectrometry (LA-ICP-MS) spot number. For the bottom images, the spot ages are given. Scale is variable between images and shown at the bottom of each image. Single spot ages are listed with 1σ uncertainties.

in these samples are at least partially dependent on the degree of grain radiation damage (Rahn et al., 2004). Notably, grains defining anomalous, old age modes exhibit the lowest eU values in a given sample. These grains exhibited eU of less than ~100–170 ppm depending on the sample. Likewise, grains defining anomalous, young age modes exhibited higher eU values, with grains with eU > 650 ppm nearly always being part of an older mode. Filtering of ZFT age distributions is discussed more on a case-by-case basis.

For AFT data, radial plots and track-length histograms were constructed to show single-grain age and track length distributions for each sample (Figs. 7B, 7C; Galbraith, 1988, 1990, 2005; Vermeesch, 2009). None of the samples pass a χ^2 test, so we report central ages (with two-standard-error uncertainties) for each sample (Galbraith, 1981, 2005; Vermeesch, 2009; Hasebe et al., 2013). Mixing calculations (Vermeesch, 2009) were used to identify possible multiple kinetic populations within samples. Although the samples are statistically inconsistent with a singular age value, most samples appear to record a common thermal history. In addition to the possibility of multiple kinetic populations in the ZFT samples, as described above, age dispersion in both the apatites and the zircons may also reflect incomplete laser ablation–inductively coupled plasma–mass spectrometry (LA-ICP-MS) measurements of uranium (and/or thorium) concentration due to unrecognized U zoning in some grains, (e.g., Vermeesch, 2017; Cogné and Gallagher, 2021).

Modeling of Thermal History

Inverse models are presented for all of the plutonic samples in this study (samples CG18-2, CG18-4, CG18-6, CG19-1, and CG18-12; see Table 3). Owing to the unusual apatite chemistry (very low eU concentrations; see Results below), the one metasedimentary sample (CG18-8) was not modeled. The models were constrained using ZFT ages, AFT ages, and AFT lengths. The filtered ZFT distributions that best reflect in situ cooling were used as model constraints. For one sample (CG18-6), bimodal AFT age distributions are separated on the basis of D_{par} (Burtner et al., 1994). Filtering of the ZFT and AFT age data is discussed in additional detail on a case-by-case basis in the Results section.

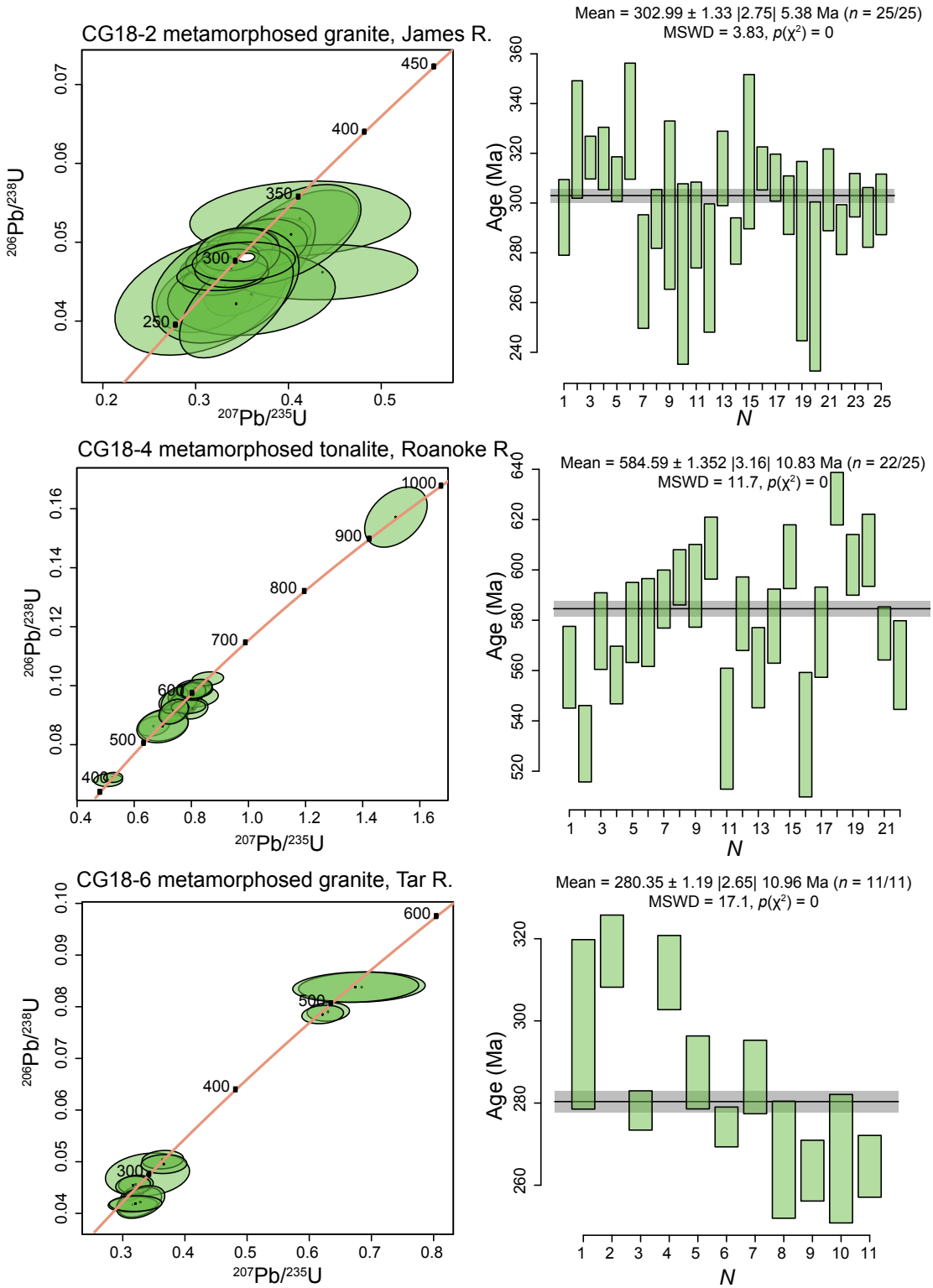

Figure 5. Concordia plots for all zircon U-Pb isotope ratio determinations. For igneous samples, concordia plots are paired with weighted mean age calculation plots; for sedimentary sample CG18-8, concordia plots are paired with zircon U-Pb age histograms. In weighted mean age plots, *n* is the number of single grain age use for the age calculation (numerator) as well as the total number of single grain measurements (denominator). In the age histogram, *n* is simply the number of single grain ages shown on the plot. On weighted mean age plots *N* along the horizontal axes gives a count of the number of ages used in the weighted mean age calculation. All plots were generated in IsoplotR (Vermeesch, 2018). MSWD—mean squared weighted deviation, R.—River. Errors in ages on weighted mean age plots are, in order, 1σ, 2σ, and 2σ × √MSWD. (*Continued on following page.*)

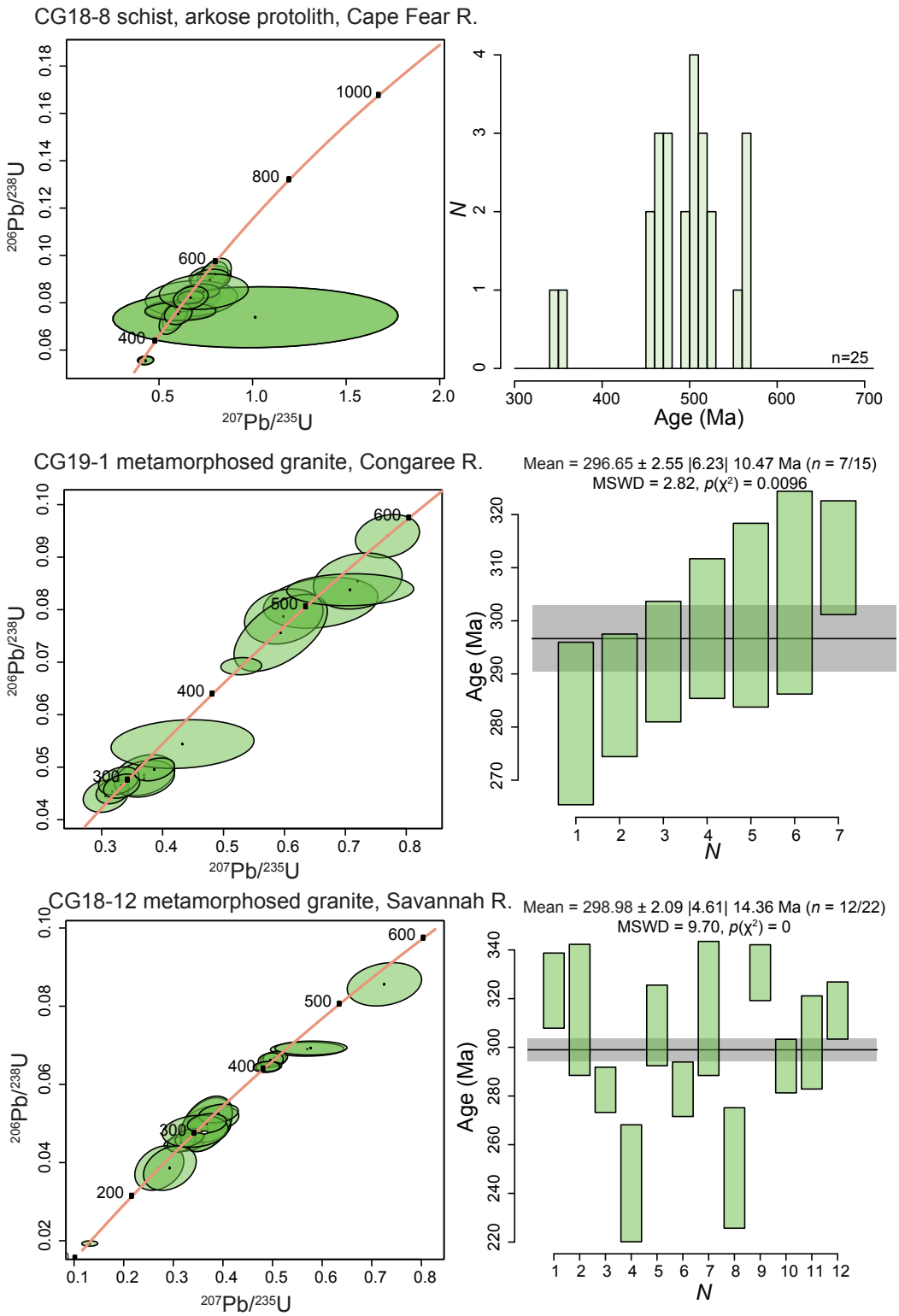

Figure 5 (*continued*). Concordia plots for all zircon U-Pb isotope ratio determinations. For igneous samples, concordia plots are paired with weighted mean age calculation plots; for sedimentary sample CG18-8, concordia plots are paired with zircon U-Pb age histograms. In weighted mean age plots, *n* is the number of single grain age use for the age calculation (numerator) as well as the total number of single grain measurements (denominator). In the age histogram, *n* is simply the number of single grain ages shown on the plot. On weighted mean age plots *N* along the horizontal axes gives a count of the number of ages used in the weighted mean age calculation. All plots were generated in IsoplotR (Vermeesch, 2018). MSWD—mean squared weighted deviation. Errors in ages on weighted mean age plots are, in order, 1σ, 2σ, and 2σ × √MSWD.

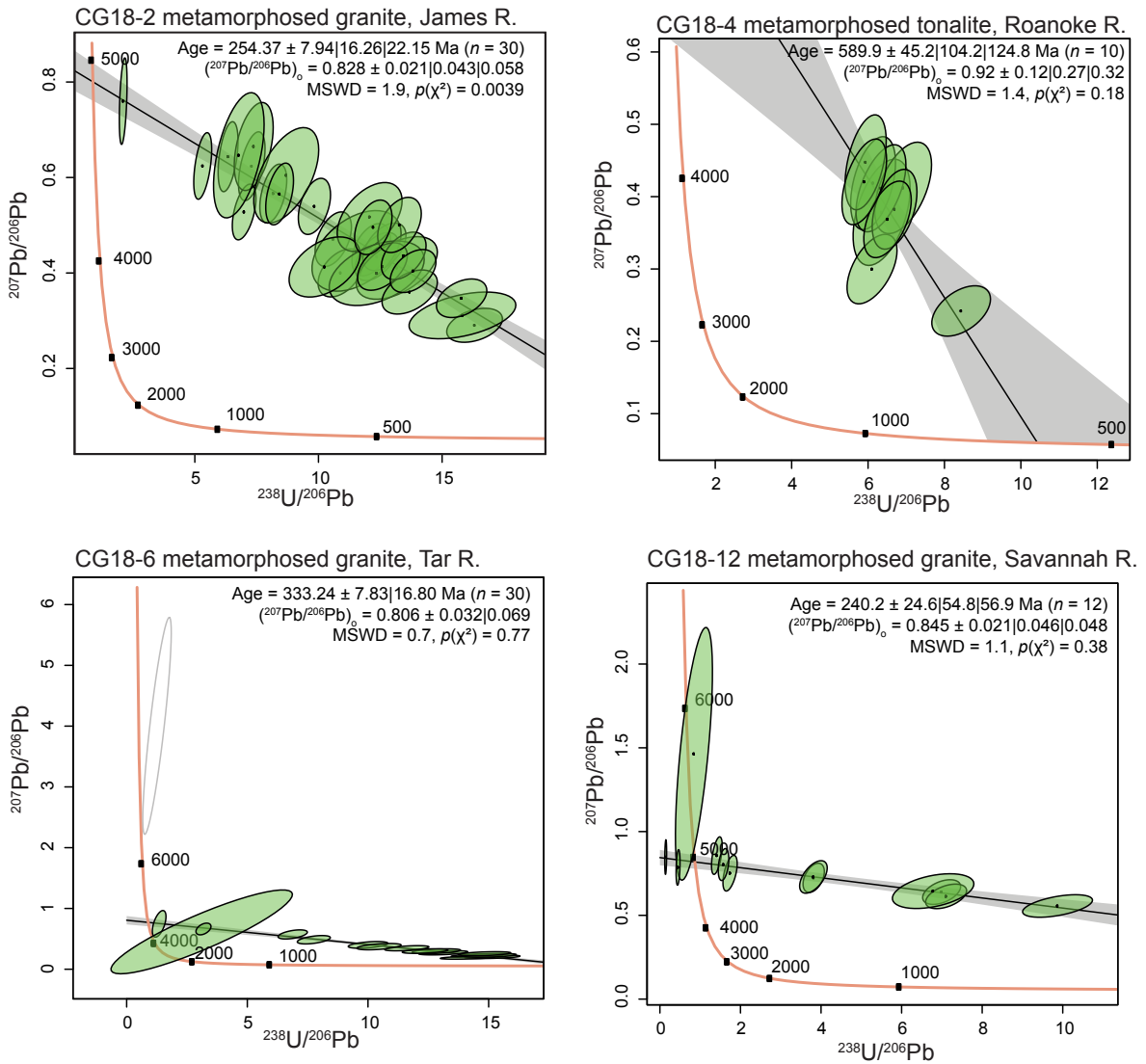

Figure 6. Tera-Wasserburg concordia plots for apatite U-Pb isotope ratio determinations. Open circles show samples not included in regressions. The *x*-intercept of the regression line shows apatite U-Pb cooling age, and *y*-intercept shows common Pb isotope ratios at the time of crystallization. All plots were generated in IsoplotR (Vermeesch, 2018). MSWD—mean squared weighted deviation, R.—River. Errors in ages on weighted mean age plots are, in order, 1σ, 2σ, and 2σ × √MSWD. The third error is not given for sample CG18-6 owing to the MSWD <1. $(^{207}Pb/^{206}Pb)_o$ is the common lead isotope ratio at the time of crystal formation. Given errors are 1σ and 2σ. Grey envelopes around regression line are 2σ error envelopes. Grey envelopes around mean age on weighted mean plots show 2σ errors.

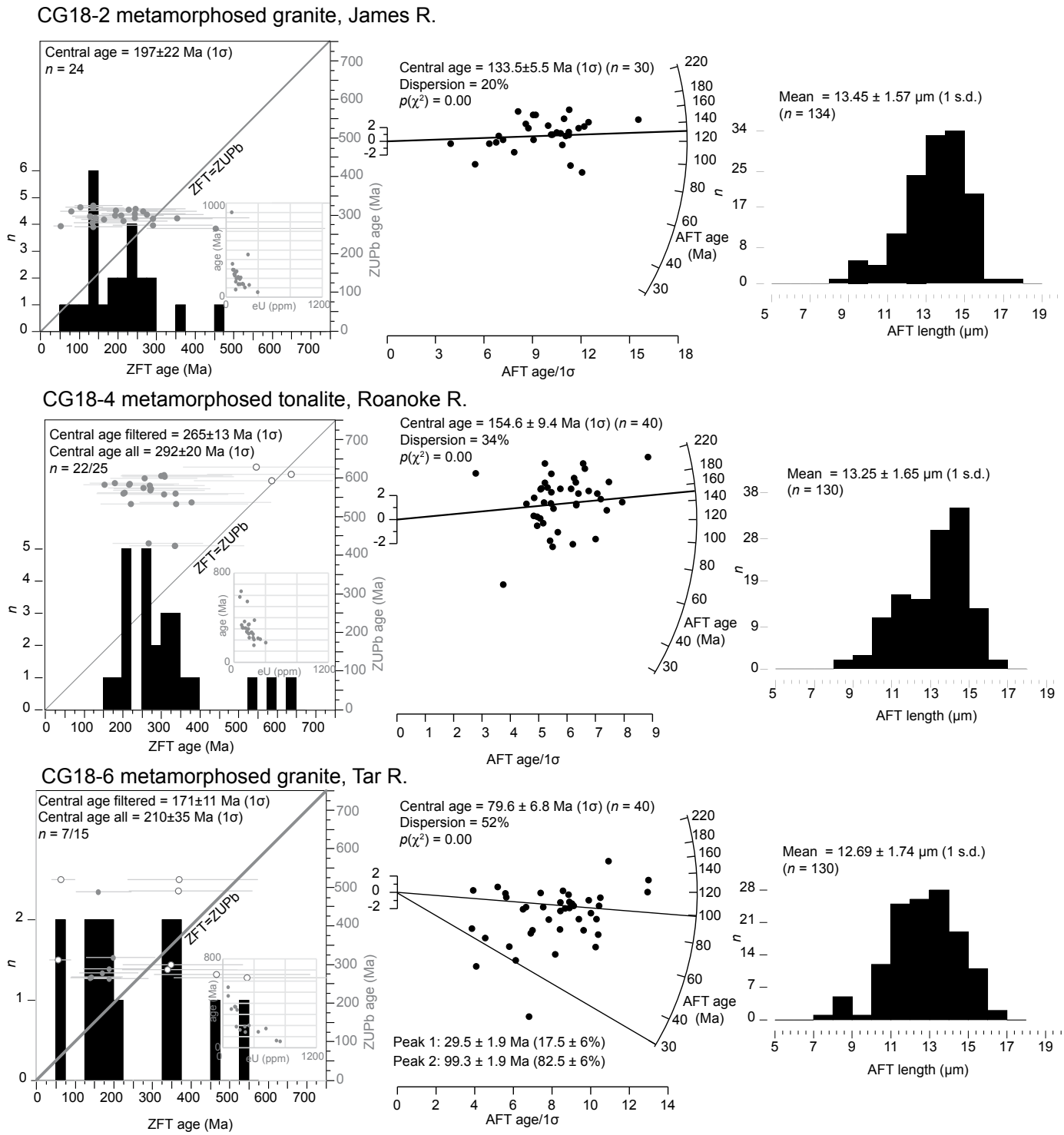

Figure 7. Apatite and zircon fission-track (AFT and ZFT, respectively) data. The left-hand column contains histograms showing ZFT age distributions. Bin width is 25 m.y. Histogram is superimposed over plot of zircon U-Pb (ZUPb) versus ZFT measurements for each single grain. The horizontal error bars on the cross plot are two standard errors. No errors are shown for the ZUPb ages because they are small relative to the size of the points on the graph. Closed circles represent ages that are interpreted to record in situ cooling and are used in filtered central age calculation; open circles represent either high effective uranium (eU), anomalously young single-grain ages, or low-eU grains that overlap the paired crystallization age measurement. Inset plots show ZFT age versus eU. The middle column contains radial plots showing AFT age data. Plots are constructed using a logarithmic transformation centered on 120 Ma. Lines from origin to right-hand age axis indicate either the central age (one line only) or else distinct age modes (multiple lines). The vertical axes on the left of the plots shows the standardized estimate of the fission track age, with the labels ±2 defining the magnitude of the 2 standard error envelope. The right-hand column contains histograms showing AFT track-length distributions. s.d. is the standard of the fission track length distribution. R.—River. All plots were constructed in RadialPlotter version 9.5 (Vermeesch, 2009). (*Continued on following page.*)

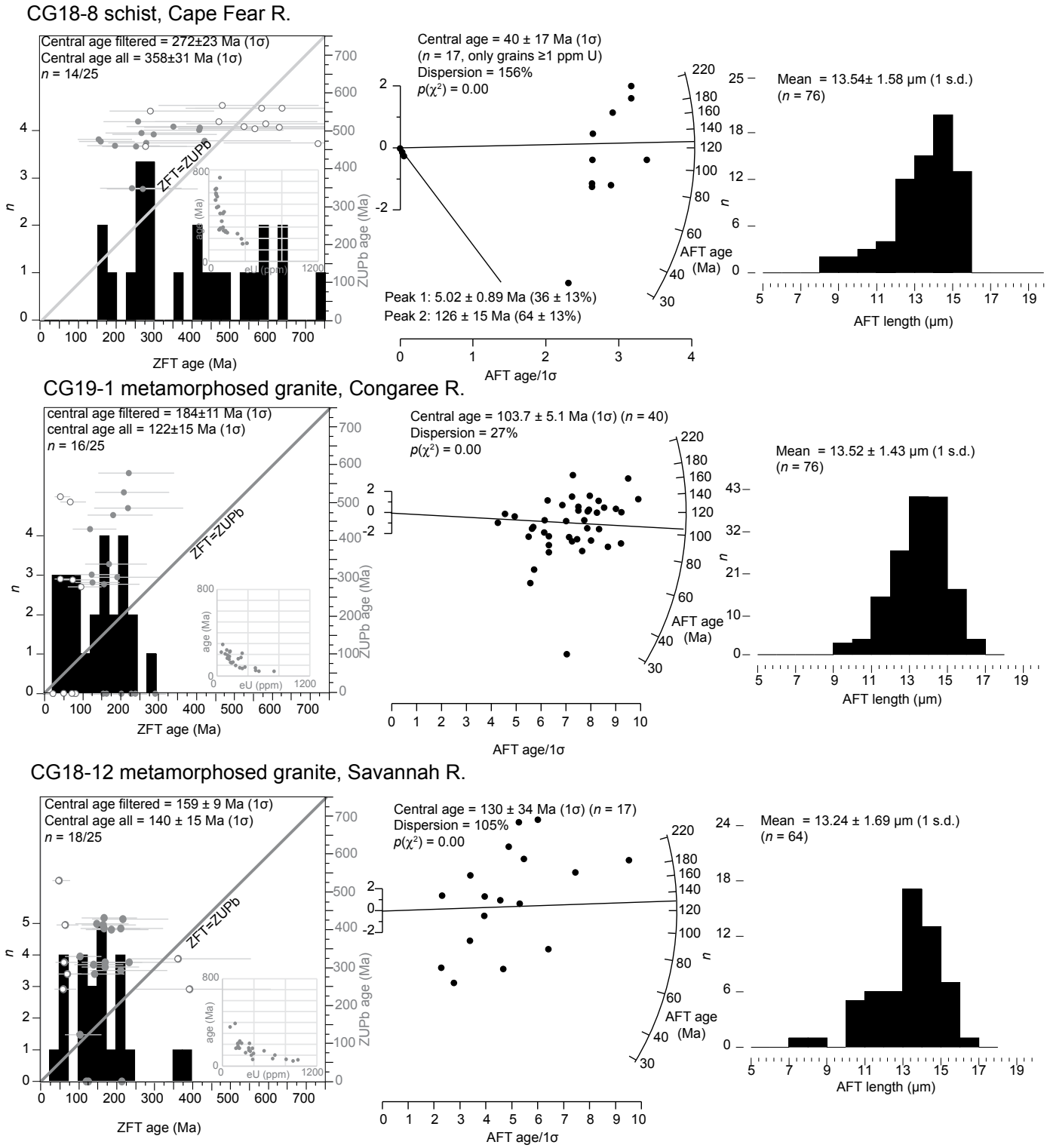

Figure 7 (*continued*).

TABLE 3. DESCRIPTION OF INVERSE AND FORWARD TIME-TEMPERATURE MODELS

1. Thermochronologic and thermal maturity data

Data used in simulations

	Inverse	Forward	Data source*
AFT ages	x	x	1
AFT lengths	x	x	1
ZFT ages	x	x	1
VR		x	2

Data treatment, uncertainties, and other relevant constraints

AFT samples are divided into multiple kinetic populations if:

(1) mixture calculations indicate multiple sample modes; and

(2) the age dispersion correlates to D_{par}.

ZFT raw age distribution is filtered to reflect only grains with typical uranium concentrations.

2. Additional geologic information

Assumption	Explanation
Initialization at 700 ± 100 °C at time of zircon U-Pb age	Crystallization temperature of granite
Intermediate cooling through 570–375°C	Pb partial retention zone for AUPb system; robust AUPb ages only
Near-surface temps and reheating; Permo-Triassic	Regional Triassic basins, possibly superimposed magmatic heating

3. System- and model-specific parameters

AFT kinetic model: Ketcham (2016).
ZFT kinetic model: Ketcham et al. (2007).
VR kinetic model: Sweeney and Burnham (1990) model of maximum VR.
Statistical fitting criteria: acceptable—all GOF statistics >0.05; good—mean GOF statistic >0.5, all GOF stats 1/(N + 1) where N is number of GOF stats.
Modeling code: HeFTy version 1.9 (Ketcham, 2016).
Number of time-temperature paths attempted: 10,000 for inverse models.
Time-temperature path characteristics: halved twice; monotonic consistent; episodic for Mesozoic heating and cooling, gradual for others.

*1—this study; 2—adapted from Malinconico (2015).

AFT—apatite fission track, AUPb—apatite U/Pb, ZFT—zircon fission track, VR—vitrinite reflectance, D_{par}—maximum etch pit diameter parallel to the crystallographic *c*-axis, GOF—goodness of fit.

The inverse models initialize at a temperature of 700 ± 100 °C at the approximate crystallization age of the pluton as recorded by the ZUPb data. For three samples that yield robust AUPb ages that are reconcilable with ZUPb data (samples CG18-2, CG18-4, CG18-12), we force the models through the apatite Pb partial retention zone (PbPRZ), which is 375–570 °C (Cochrane et al., 2014), at the time of the AUPb cooling age. A phase of exhumational cooling to near-surface temperatures by ca. 230 Ma (the timing of the earliest sediment accumulation in the Triassic basins of the region) is imposed on the models. The models then require heating at the time of Triassic sedimentation (ca. 230–215 Ma) and subsequent exhumational cooling, with potential for a wide range of maximum paleotemperatures and for the heating-cooling transition to occur within a broad time window. Present-day temperatures are estimated to be 10 ± 10 °C.

The ZFT and AFT annealing kinetics of Ketcham (2016; see also Yamada et al., 2007) and Ketcham et al. (2007), respectively, are used in the models. The zircon annealing kinetics model was developed for zircons with some radiation damage from spontaneous fission tracks and should therefore be more appropriate than other extant models for undamaged zircon (e.g., Rahn et al., 2004). The selected ZFT kinetic model has a predicted closure temperature of 282 °C at cooling rates of 10 °C/m.y. All paths between constraint boxes in time-temperature space were halved twice and treated as "monotonic consistent" (e.g., no cooling path segments when a phase of heating is prescribed in time-temperature space). The initial Paleozoic cooling phases are treated as gradual. Owing to the possibility of magmatic heating that may or may not have been superimposed over burial heating in the Mesozoic (e.g., Kohn et al., 1993), the randomization style was set to episodic for the Mesozoic portion of the model phase.

A model is considered "good" if two conditions are met. First, the mean goodness of fit (GOF) value

must be at least 0.5. Second, the minimum GOF value must be greater than 1/(*N* + 1), where *N* is the number of GOF tests that were run. A model is considered "acceptable" if all GOF values are >0.05 (Ketcham, 2016). The models were iterated until they identified 20 good time-temperature paths.

In addition to the inverse modeling described above, a suite of forward time-temperature models for sample CG18-2 (James River) is presented. The site from which this sample was taken is the best constrained, overall, in terms of thermal maturity data (e.g., Durrant, 1979; Tseng et al., 1996; Malinconico, 2015; this study) and has a clear spatial association with a Triassic basin (Fig. 2). The design of this model is similar to that of the inverse models (e.g., see Table 3). However, it is specifically designed to evaluate the degree of heating that occurred in the Triassic Period. Because the model involves more geological interpretations and assumptions, it is presented in the Discussion section.

RESULTS

Sample CG18-2: Metamorphosed Granite, Petersburg Granite, James River, Virginia

Sample CG18-2 was collected where the James River crosses the Fall Line in Richmond, Virginia, from a Carboniferous–Permian metamorphosed granitic pluton called the Petersburg Granite (Figs. 2, 3). The pluton is bordered to the west by Richmond Basin and to the east by Cretaceous–Cenozoic passive-margin deposits (Fig. 2). The preserved portion of Richmond Basin is bound by steeply dipping normal faults (Schlische, 2003). The youngest preserved strata in Richmond Basin are Carnian. They are slightly older than the youngest preserved strata in basins along strike to the north and south (e.g., Taylorsville Basin, Deep River Basin), which are Norian (Olsen, 1997). Malinconico (2015) reported VR measurements of 0.69% in the VAGO-1 core at ~50 m depth in portions of Taylorsville Basin along structural strike to the north and documented ~1–3 km of post-Triassic erosion based on VR versus depth relationships.

Most zircon grains from this sample are euhedral and elongate with aspect ratios of ~4:1. Post-analysis CL imaging demonstrates that all grains exhibit oscillatory zoning and are similarly bright in CL (Fig. 4). A subset of grains have rims that are darker in CL and more strongly etched. The darker rims do not embay cores, suggesting the zoning is magmatic rather than reflecting later replacement. This interpretation is supported by the fact that most ZUPb isotope ratio values overlap with the concordia line at 2σ. The sample yields a weighted mean zircon $^{206}Pb/^{238}U$ age of 303 ± 5 Ma that we interpret to reflect the timing of crystallization (Fig. 5). This is consistent with geologic mapping (Marr, 2002). It is also in reasonably good agreement with the ages determined by chemical abrasion–thermal ionization mass spectrometry of 296 Ma from the same outcrop and 300 Ma for an outcrop ~20 km to the west (Owens et al., 2017). The single-grain AUPb data clearly define a discordia line and suggest cooling through the PbPRZ at ca. 254 ± 16 Ma (Fig. 6). The data also suggest a common $^{207}Pb/^{206}Pb$ ratio of ~0.8 at the time of crystallization, which is close to lead isotope ratios measured in low-uranium minerals that formed in the late Paleozoic (Stacey and Kramers, 1975).

The sample yields a unimodal ZFT age distribution (Fig. 7) with a central age of 197 ± 22 Ma. Owing to the unimodal character of the ZFT age distribution, no single grain age measurements were filtered. The AFT age distribution exhibits a central value of 133.5 ± 5.5 Ma (Fig. 7). The mean track length is 13.45 ± 1.57 µm. The ZFT and the AFT age and length distributions were used in the inverse and forward modeling, and none of the data were filtered or subdivided into kinetics populations for this purpose.

Sample CG18-4: Metamorphosed Tonalite, Roanoke Rapids Complex, Roanoke River, North Carolina

Sample CG18-4 is a weakly metamorphosed tonalite that was collected where the Roanoke River crosses the Fall Line near the towns of Weldon and Roanoke Rapids in North Carolina (Figs. 2, 3). The rock unit has been mapped as part of the Roanoke Rapids terrane (North Carolina Geological Survey, 1985; Weems et al., 2009). Typical zircon grains from this sample are euhedral and equant with aspect ratios of ~2:1. Post-analysis CL imaging demonstrates that the vast majority of grains show similar brightness in CL and exhibit oscillatory, but broad, bands of CL zoning (Fig. 4). A small subset of grains (<5%) are anomalously bright in CL. Twenty-two (22) of 25 analyses are distributed across an ~100 m.y. range, from 535 to 628 Ma. Given their consistent CL characteristics and the relatively low precision of the ages, we interpret these analyses to reflect a single age of zircon crystallization and calculate a weighted mean age of 585 ± 11 Ma (Fig. 5). We consider the pluton to be approximately Ediacaran, and additional work is required to further refine this age. The Ediacaran age is consistent with the age constraints summarized by Hibbard et al. (2002). Two anomalously bright CL grains yield young Silurian ages and likely reflect metamorphic growth. A single age of ca. 938 Ma is interpreted to reflect inheritance. The AUPb lower intercept age is imprecise (590 ± 104 Ma) but also approximately Ediacaran (Fig. 6).

The overall ZFT age distribution has a central value of 292 ± 20 Ma (Fig. 7). On the age histogram, three grains appear to define a distinct, older age mode that is Neoproterozoic or earliest Palezoic and overlapping with paired ZUPb age measurements. We filter out these three single grain ages and also note that they exhibit low eU values as described above (75, 91, and 170 ppm). The remainder of the ZFT age distribution is fairly homogeneous, younger than paired ZUPb measurements, and yields a central age of 265 ± 13 Ma. For these reasons, the three older, outlying grains are excluded from inverse modeling. The AFT age distribution yields a central value of 154.6 ± 9.4 Ma and does not obviously reflect a mixture of multiple age modes. The apatite fission tracks are shorter than at the James River site, with a mean track length of 13.25 ± 1.65 µm.

Sample CG18-6: Carboniferous–Permian Granitic Pluton, Tar River, North Carolina

Sample CG18-6 is a weakly metamorphosed granite sample that was collected near where the

Tar River crosses the Fall Line in the town of Rocky Mount, North Carolina (Figs. 2, 3). An age of 320–270 Ma, or approximately Carboniferous–Permian, is assigned to the pluton (North Carolina Geological Survey, 1985), and an earliest Carboniferous (345 Ma) Rb-Sr age has been reported (Gay, 2004). Typical zircon grains from this sample are euhedral and elongate with aspect ratios of ~4:1. The vast majority of these grains are dark in CL and are strongly etched in ZFT mounts, though rare bright CL grains are present (Fig. 4). Zircon U-Pb ages in our sample broadly define two age distributions, one from 317 to 264 Ma (n = 11) and an older distribution defined by fewer grain analyses from 519 to 487 Ma (n = 4) (Fig. 5). There is no obvious relationship between CL response, grain morphology, and age. Previous interpretations of the composition and of Nd, Sr, and Pb isotopic data of Carboniferous–Permian plutons suggest that they are derived from anatexis of crustal material (Samson et al., 1995). In light of these interpretations, we consider the younger age distribution to be representative of the approximate crystallization age (weighted mean zircon $^{206}Pb/^{238}U$ age of ca. 280 ± 11 Ma), with the older population representing xenocrystic material. The sample yields an AUPb age of ca. 333 ± 17 Ma (Fig. 6). This age is slightly older than the ZUPb age but is broadly consistent with rapid cooling to below the closure temperature for Pb diffusion in apatite following intrusion.

The sample ZFT age distribution exhibits a central value of 210 ± 35 Ma (Fig. 7). However, the ZFT age distribution is clearly heterogeneous. The largest cluster of ZFT cooling ages is between 201 and 142 Ma. These ages are younger than paired ZUPb measurements and broadly similar to the in situ ZFT ages at the two sites to the north. Although there is a limited number of single grain ZFT ages, the sample appears to exhibit two other age modes, a <100 Ma mode defined by two grains and an older mode defined by grains with ZFT ages similar to or older than paired ZUPb measurements. Notably, the two young grains exhibit some of the highest eU values measured in this study (687 and 735 ppm). The youngest age mode is defined by six of the seven grains with the lowest eU values of the sample, which generally are <170 ppm. The AFT age distribution is also heterogeneous, with a central value of ca. 80 Ma. About 83% of grains define an age mode around 99.3 ± 1.9 Ma, and the remainder define a younger late Cenozoic age mode. Apatite fission tracks in this sample are shorter than at other sites (12.69 µm) and show a high degree of dispersion (standard deviation of 1.74 µm) compared to other samples in this study.

Sample CG18-8: Neoproterozoic–Cambrian Schist, Cape Fear River, North Carolina

Sample CG18-8 was collected where the Cape Fear River crosses the Fall Line to the east of the major Triassic extensional Sanford Basin (Fig. 2). Bedrock here is Neoproterozoic–Cambrian schist and gneiss (Fig. 3; North Carolina Geological Survey, 1985). The sample is a plagioclase-quartz-mica-garnet schist. Typical zircon grains from this sample are equant, have irregular morphology, and are bright in CL and exhibit oscillatory zoning (Fig. 4). The sample exhibits a broad ZUPb age distribution between 567 and 460 Ma (Fig. 5). It also exhibits two concordant ages of ca. 350 Ma, which may record the growth of metamorphic zircon. The youngest age population defined by more than two grains has a weighted mean age zircon $^{206}Pb/^{238}U$ of ca. 485 Ma, and this is interpreted to be the maximum depositional age for this unit (Dickinson and Gehrels, 2009).

The ZFT age distribution is heterogeneous, likely characterized by at least two distinct groups of grains (Fig. 7). There is a gradation between low-eU grains whose ZFT ages clearly reflect the crystallization ages of detrital zircons versus higher-eU grains whose ZFT age reflects exhumational cooling, so rather than visually differentiating between these two groups, we define a cutoff of 125 ppm eU based on age-eU relationships observed in other samples. The younger of the two age distributions, which is defined by ~50% of the total grains, exhibits an age mode of 272 ± 23 Ma. The older, low-eU grains are excluded from inverse modeling.

Overall, sample CG18-8 exhibits a central AFT age of 40 ± 17 Ma. However, the age distribution is clearly bimodal, with an older age mode of 126 ± 15 Ma and a younger mode that is 5.0 ± 0.9 Ma. The grains also exhibit some unusual compositional attributes. Twenty-one (21) grains exhibit eU concentration of <1 ppm. Ten (10) of these 21 grains exhibit AFT ages of 0 Ma. Most of the remaining 19 grains have low eU concentrations (16 grains with eU of 1–10 ppm), and three have higher uranium concentrations. The grains are also characterized by very low D_{par}, with a mean value of 1.63 µm. The sample exhibits fission tracks that are relatively long in the context of the overall sample set, with a mean value of 13.54 ± 1.58 µm. Owing to the anomalous low eU concentrations and D_{par} of the apatite analyses and the numerous grains with no spontaneous fission tracks, we do not present an inverse thermal model for this sample.

Sample CG19-1: Columbia Granite, Congaree River, South Carolina

Sample CG19-1 was collected near the Fall Line of the Congaree River from a metamorphosed granite pluton (Figs. 2, 3). Typical zircon grains from this sample are euhedral with aspect ratios of ~3:1. The majority of these grains are dark in CL and are strongly etched in ZFT mounts (Fig. 4). A subset of grains has bright-CL cores. In addition to regional evidence for derivation of Carboniferous–Permian plutons from melting of continental crust (Samson et al., 1995), ZUPb isotope ratios from nearby plutons in the South Carolina Piedmont as well as across the Georgia Piedmont show evidence for significant incorporation of xenocrystic zircons (Dallmeyer et al., 1986; Mueller et al., 2011). Our sample yielded a range of ZUPb ages, with a younger age distribution of ca. 341–281 Ma and an older age distribution of ca. 579–432 Ma (Fig. 5). There are no obvious relationships between CL response, grain morphology, and age. From the younger age distribution, we calculate a weighted mean $^{238}U/^{206}Pb$ age of 297 ± 10 Ma, which overlaps with a Rb-Sr age of 285 ± 7 Ma (1σ) reported for the pluton (Fullagar and Butler, 1979). Following previous geochronologic studies in this province, we assume that the older ages are xenocrystic.

The overall ZFT age distribution exhibits a very young central age of 122 ± 15 Ma. However, there is clearly a distinct, young ZFT age mode (Fig. 7). Although the young distribution includes grains with very high eU concentrations (737, 1227 ppm), it also includes grains with eU concentrations down to 241 ppm. These younger high-eU grains are excluded from inverse modeling, and the filtered ZFT age distribution exhibits a central age of 184 ± 11 Ma. The AFT age distribution is relatively homogeneous, yielding a central age of 104 ± 5 Ma. The sample exhibits apatite fission tracks with a mean value of 13.52 ± 1.43 µm, making it similar to most of the samples to the north.

Sample CG18-12: Unnamed Gneiss, Savannah River, South Carolina–Georgia

Sample CG18-12 was collected near the Fall Line of the Savannah River from a metamorphosed and sheared granitic rock that is mapped as being part of a unit of undifferentiated Precambrian–Paleozoic gneisses, schists, granites, and phyllites (Figs. 2, 3; Lawton et al., 1976). Typical zircon grains from this sample are subhedral, bright in CL images, and exhibit oscillatory zoning (Fig. 4). Several grains have bright-CL cores that appear to have been fractured and healed by dark-CL zircon. Like the other Pennsylvanian–Permian pluton samples from the Carolinas, the ZUPb ages are highly heterogeneous. The sample exhibits two distributions of concordant ages of 440–400 Ma and 340–240 Ma (Fig. 5). Similarly to other samples, we interpret the older ages to be from xenocrystic zircon and the younger ages to reflect the time of crystallization. The young ages yield a weighted average $^{206}Pb/^{238}U$ age of 299 ± 14 Ma, which we interpret to be the approximate crystallization age. The AUPb intercept age is ca. 240 Ma (Fig. 6).

The ZFT age distribution of this sample is heterogeneous (Fig. 7). Most single-grain ages cluster near the central age of 140 ± 15 Ma. However, similarly to samples described above, anomalous young and old age distributions are evident. These age distributions include grains that exhibit the highest and lowest eU values of the sample and they are filtered. The central age of the filtered ZFT is 159 ± 9 Ma. The AFT age distribution is also highly dispersed but does not clearly exhibit multiple age modes. It has a central value of 130 ± 34 Ma that is similar to that of other samples in this study. The sample exhibits a mean fission-track length of 13.24 ± 1.69 µm that is intermediate between values measured at other sites to the north.

Inverse Modeling

Each of the five igneous samples is compatible with a thermal history involving rapid cooling (>10 °C/m.y.) from pluton-emplacement temperatures to near-surface temperatures by the Triassic, reheating starting in the Triassic (>10 °C/m.y.), and rapid Jurassic–Early Cretaceous cooling (1–10 °C/m.y.) followed by slower cooling (~1 °C/m.y.) (Fig. 8). The models indicate Triassic–Jurassic heating to temperatures of >300 °C, although there are tradeoffs between the maximum paleotemperature and the time at which it occurred. Lower maximum paleotemperatures (e.g., 300–250 °C) are in some cases permissible for models that achieve maximum paleotemperatures later in time (e.g., in the Early Cretaceous as opposed to the Triassic or Jurassic). From north to south, the models indicate cooling below 282 °C (approximate closure temperature of ZFT) mostly in the Jurassic. Based on good model fits, this occurs between ca. 200 and 150 Ma at the James River site (sample CG18-2), between ca. 230 and 160 Ma at the Roanoke River site (CG18-4), between ca. 200 and 140 Ma at the Tar River site (CG18-6), between ca. 190 and 140 Ma at the Congaree River site (CG19-1), and between ca. 180 and 140 Ma at the Savannah River site (CG18-12). From north to south, based on good model fits, cooling below 116 °C (approximate closure temperature of AFT) occurs in the Jurassic (for northern sites) or slightly later in the Early Cretaceous (for southern sites), with the transition to slower cooling rates lagging by tens of millions of years. Specifically, this occurs at 160–140 Ma (sample CG18-2; James River), 180–150 Ma (CG18-4; Roanoke River), 120–90 Ma (CG18-6; Tar River), 130–100 Ma (CG19-1; Congaree River), and 150–120 Ma (CG18-12; Savannah River). This north-south gradient in cooling is also mirrored by the empirical AFT ages. All sites indicate residence below ~80 °C since 80 Ma (and all but sample CG18-6 [Tar River] since 120–100 Ma) and slower cooling in that time window. The Tar River (sample CG18-6) model indicates a phase of accelerated cooling in the Neogene.

DISCUSSION

Forward Model of Time-Temperature History

The early Mesozoic paleotemperatures caused by Triassic–Jurassic heating for sample CG18-2 (Petersburg Granite, James River, Virginia) in the inverse model (Fig. 8) are 300 °C or more. Although some burial heating in the proximal hanging wall of the Richmond Basin bounding fault system seems likely, the modeled temperatures are incongruent with shallow VR measurements (sample depths of hundreds of meters) in the Richmond Basin of ~0.7%. These VR measurements indicate Triassic peak burial temperatures on the order of 100 °C (Malinconico, 2015) and therefore limit post-Triassic cooling to <100 °C (see also Roden and Miller [1991] and Tseng et al. [1996] studies of Taylorsville Basin). Triassic–Jurassic paleotemperatures of >300 °C are also indicated for other sites to the south, and, although the thermal histories of those sites are not as well constrained, this magnitude of heating does not seem congruent with published VR data to the south (e.g., Reid and Milici, 2008).

To better reconcile the fission-track and VR observations, we constructed a suite of forward models for sample CG18-2 (Fig. 9) that is similar to the inverse models in terms of the overall patterns of cooling and heating through time (Table 3). The forward models differ from the inverse models in that they are designed to explore five different magnitudes of Triassic heating, ranging from 360 °C down to 120 °C in 60 °C increments, while holding all other aspects of the thermal history equal. The range of maximum paleotemperatures reflects the fact that for hold times of 1–10 m.y. and at relevant heating rates, most inherited zircon fission tracks

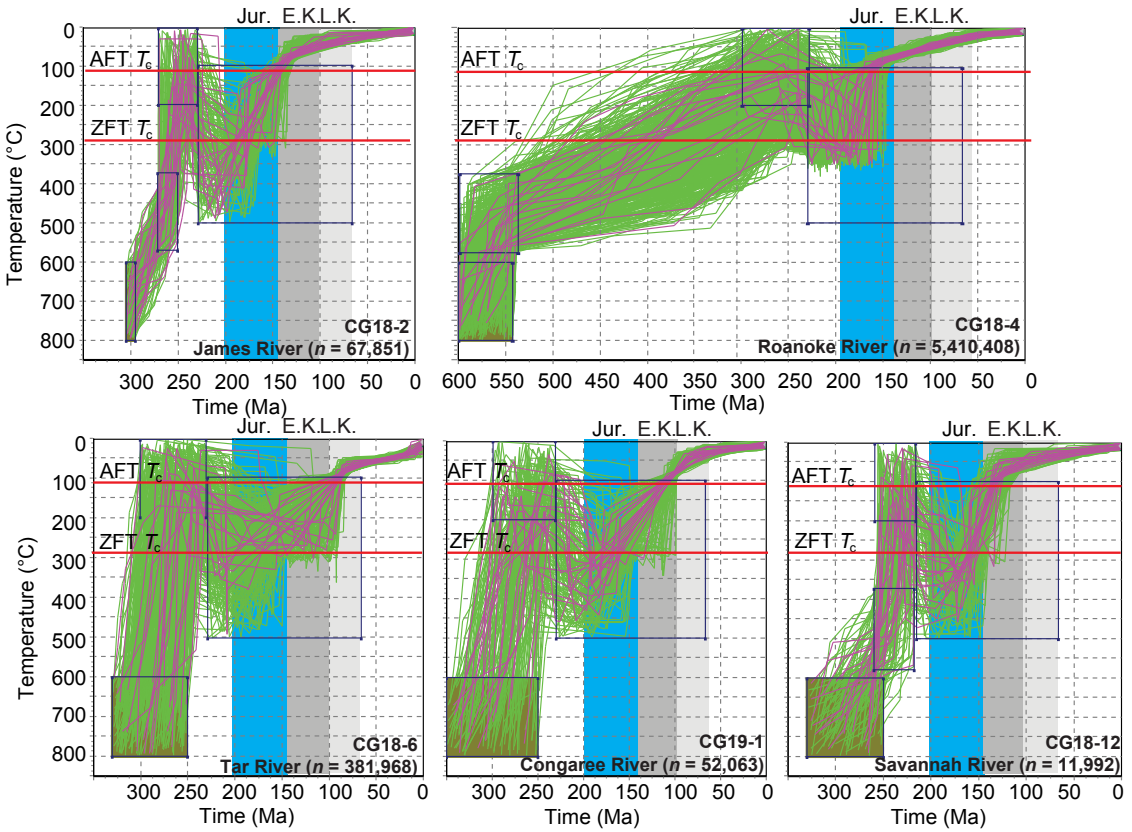

Figure 8. Inverse models of time-temperature history recorded by the samples. Models are constrained by zircon fission-track (ZFT) age and apatite fission-track (AFT) age and length data. Constraints in time-temperature space are given in Table 3. Pink paths are good time-temperature paths, whereas the green paths are acceptable time temperature paths (see text for definitions of "good" and "acceptable"). The blue, dark gray, and light gray bars show the Jurassic (Jur.), Early Cretaceous (E.K.), and Late Cretaceous (L.K.), respectively. The red lines show the closure temperatures (T_c) for ZFT and AFT. All models were generated in HeFTy version 1.9 (Ketcham, 2005). Number of model iterations to obtain 20 good model fits is indicated along with sample number label.

are annealed at maximum burial temperatures of ~300 °C or more given the ZFT annealing kinetics described above (see also Reiners and Brandon, 2006). However, at lower maximum paleotemperatures, the ZFT system is only partially reset, with fission-track annealing occurring at temperatures as low as 170 °C or lower (Reiners and Brandon, 2006). Thus, the forward models evaluate the degree to which partial resetting of the ZFT system is applicable to the field site of this sample.

Like the inverse models, the forward models involve (1) cooling to near-surface temperatures by ca. 250 Ma, (2) heating starting at 230 Ma (the time of earliest sediment accumulation in Richmond and Taylorsville Basins), (3) a transition from heating to cooling at 200 Ma (a time that should be considered approximate given the inverse modeling and the variability of reported ZFT ages around the CG18-2 site; see Durrant, 1979; Roden and Miller, 1991; Fig. 1), (4) rapid cooling to below the AFT closure temperature until 120 Ma, and (5) slower cooling after 120 Ma. The forward model predicts VR (mean maximum reflectance through 360° rotation under polarized light) using a kinetic model (Sweeney and Burnham, 1990; called "EASY%Ro"). Whereas the granite sample lacks any vitrinite, the VR prediction could be thought of as pertaining to Triassic strata that would have likely covered the Petersburg Granite, or else to vitrinite-bearing strata at an equivalent structural depth.

Only the model scenario involving maximum paleotemperatures of 360 °C (and thus complete resetting of the ZFT system) yields ZFT ages that are comparable to the empirical data based on the fitting statistics in the model. ZFT ages in all other forward model scenarios are too old (Fig. 9). The forward model scenarios involving Triassic burial heating to 360–240 °C predict AFT age and length values that are similar to empirical measurements. However, they also predict VR values (4.7%–3.4%, respectively) that are much higher than measured values in the preserved, albeit shallow, strata in Richmond Basin and also higher than those of recycled vitrinite in Cretaceous strata offshore of the Georgia coast, which mostly range from 0.7%

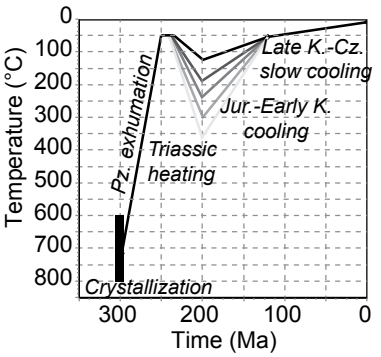

	ZFTA (Ma)	AFTA (Ma)	AFTL (µm)	SD (µm)	VR (%)
Empirical	197	134	13.5	1.6	0.7
120 °C	270	153	13.1	1.9	0.8
180 °C	268	138	13.4	1.7	1.7
240 °C	260	132	13.5	1.6	3.4
300 °C	244	129	13.6	1.5	4.6
360 °C	186	126	13.6	1.5	4.7

Figure 9. Forward model suite for sample CG18-2, collected near Richmond, Virginia, where the James River crosses the Fall Line. Model is designed to evaluate the optimal magnitude of Triassic burial heating. Table to the right compares five different maximum Triassic burial scenarios to empirical data. The model was generated in HeFTy version 1.9 (Ketcham, 2005). See text for additional details. Pz.—Paleozoic; Jur.—Jurassic; K.—Cretaceous; Cz.—Cenozoic; ZFTA, AFTA—zircon and apatite fission-track age, respectively; AFTL—apatite fission-track length; SD—standard deviation; VR—vitrinite reflectance.

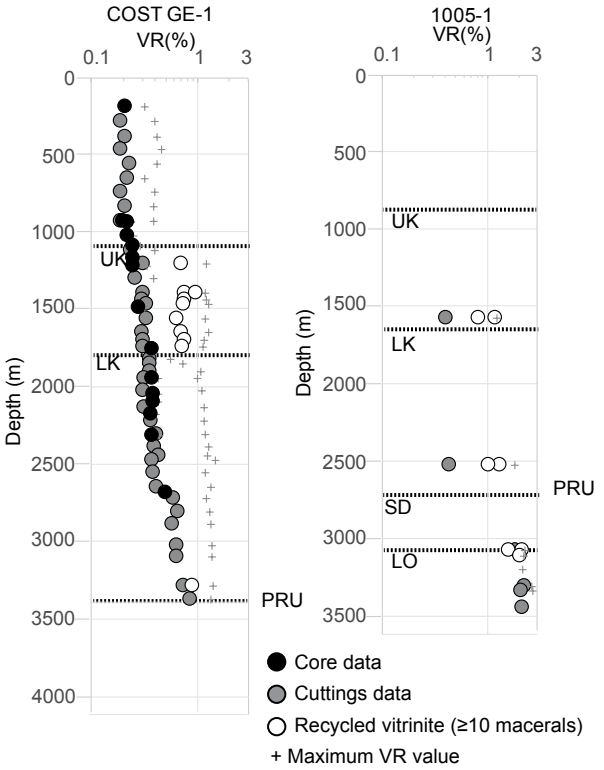

Figure 10. Vitrinite reflectance (VR) versus borehole depth in wells offshore of Georgia (see Fig. 1 for well locations). VR data are from geochemistry reports from the U.S. Bureau of Ocean Energy Management. Recycled vitrinite data are limited to peaks defined by 10 or more macerals. Tops are constrained by paleontological data and well geophysical log correlation: UK—upper Cretaceous; LK—lower Cretaceous; SD—Silurian–Devonian; LO—lower Ordovician; PRU—post-rift unconformity.

to 2% (Fig. 10). In contrast, the scenario involving burial heating to 180 °C yields VR predictions that are in better agreement with regional observations (1.7%). The AFT age and length predictions for this magnitude of heating are similar to empirical data (based on model fitting statistics). Lesser amounts of burial heating (e.g., to 120 °C) predict AFT age and length values that are too old and too short, respectively, and inconsistent with empirical measurements. In terms of the empirical AFT data, in situ VR in Triassic strata, and recycled VR in Cretaceous strata, Triassic burial heating to 180 °C (plus or minus tens of degrees) would seem to be the optimal scenario.

The thermal maturities implied by the empirical ZFT and VR data could be reconciled if the annealing kinetics model were underestimating the degree of fission-track annealing in the upper part of the ZFT partial annealing zone (PAZ), perhaps owing to a high degree of radiation damage in these zircons (e.g., Rahn et al., 2004). Nevertheless, given an array of annealing kinetics in zircons, prolonged residence in the ZFT PAZ should result in high ZFT age dispersion. This is consistent with the dispersed empirical ZFT ages, which are inversely correlated to the eU concentration of the grain. Thus, at least conceptually, the dispersed ZFT age distributions are compatible with the forward model scenario involving ~180 °C of burial heating even if the model ages exceed the measured value.

We propose that a thermal history similar to that of the forward model for sample CG18-2 (the 180 °C burial scenario) would be broadly applicable to the sites to the south, and the geologic history corresponding to the proposed thermal history is depicted schematically on Figure 11 based on the uniformity of the inverse model results. One subtle difference is that the sites to the south may exhibit slightly later cooling through the AFT closure temperature (Early Cretaceous, as opposed to Jurassic). Although the James River site (sample CG18-2) is likely to have been buried by Triassic strata, other sites around the region may have been buried by either rift or sag-phase strata as well. However, the generally high degree of ZFT age dispersion at the southern sites is consistent with a history of

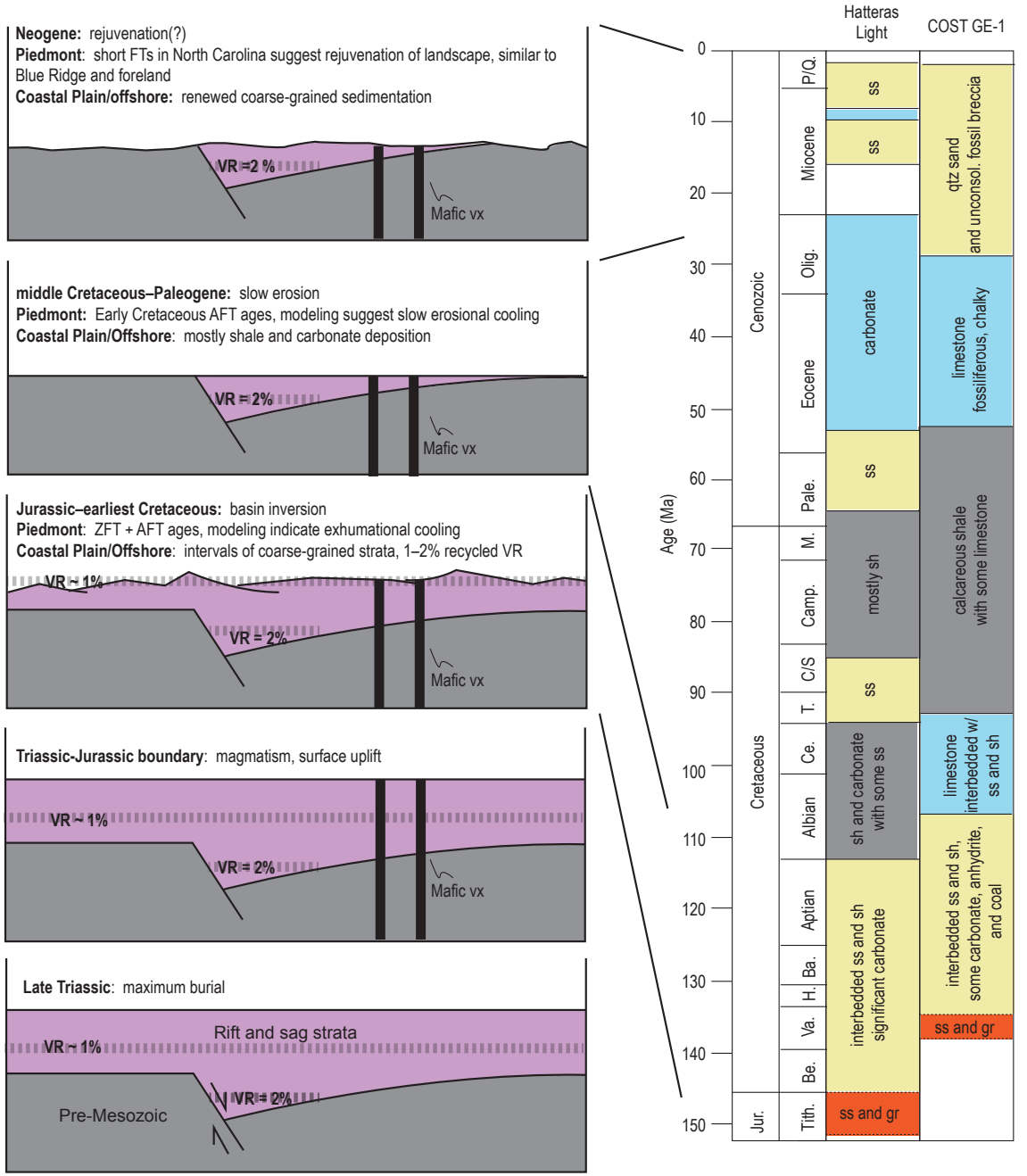

Figure 11. Schematic summary of geological controls on the thermal history of thermochronological samples. Simplified lithostratigraphy of COST GE-1 well is from Scholle (1979); lithostratigraphy of Hatteras Light well is simplified from Brown et al. (1972). See text for additional details. (A/Z) FT—(apatite/zircon) fission track, vx—volcanics, VR—vitrinite reflectance. gr—gravel, ss—sandstone, sh—shale, qtz—quartz.

prolonged holding in the ZFT PAZ, and the implied thermal maturity of Triassic basins is also consistent with recycled VR offshore as described above.

In general, we attribute most of the rapid Jurassic–Early Cretaceous cooling to exhumation. This interpretation is suggested by the lack of a preserved Jurassic–Early Cretaceous section beneath onshore areas of the Atlantic margin (e.g., see Cenomanian–Turonian onlap on Fig. 1; earlier Cretaceous and Jurassic onlap occurs farther downdip). Across most of the field area discussed in this paper, the oldest post-Triassic strata preserved below the updip portions of the coastal plain are approximately Coniacian–Santonian (Owens and Gohn, 1985), although there are Cenomanian–Turonian strata preserved beneath portions of the northern Virginia coastal plain (Fig. 1; Owens and Gohn, 1985). These observations are consistent with latest- or post-Triassic inversion of the updip portions of the coastal plain (Withjack et al., 1998) with no subsidence until the middle part of the Cretaceous. These Jurassic–Early Cretaceous stratal intervals, however, should be preserved down depositional dip (Dillon and Popenoe, 1988). We also note that cooling owing to dissipation of magmatic heat (e.g., related to the Central Atlantic magmatic province at ca. 200 Ma) may have been superimposed on top of exhumational cooling.

Lastly, we highlight that the proposed transition from rapid exhumational cooling to slower exhumational cooling overlaps temporally with a change in the grain size of sediment delivered to downdip stratigraphic sections. Jurassic–lowermost Cretaceous sections near Cape Hatteras and offshore of Georgia exhibit a high proportion of sandstone beds, whereas younger Cretaceous and Paleogene strata tend to be progressively finer grained, with widespread carbonate deposition by the Eocene (Fig. 11).

Drivers of Landscape Evolution and Basin Inversion

The post-Paleozoic geomorphic history of the Atlantic margin has been interpreted as a history of escarpment retreat as high-standing rift-related topography was progressively eroded from east to west by headward erosion (Spotila et al., 2004), although this model has not been fully tested. This escarpment-retreat model predicts a zone of maximum erosion and young cooling ages proximal to the modern escarpment. Cooling ages are predicted to increase away from this zone, both in the direction of the escarpment and toward the coast. To date, the key thermochronologic evidence in support of this model has been AHe data from the North Carolina–Virginia border portion of the western Piedmont province, which show a west-to-east decrease across the areas closest to the modern escarpment over a spatial scale of ~60 km (Figs. 1, 12). Although AFT data are also reported from that region, any spatial gradients in cooling ages are not as well resolved.

The degree to which cooling ages also increase toward the coast and away from the zone of minimum cooling ages is one aspect of the escarpment-retreat model that is not well constrained (Figs. 1, 12), despite the larger spatial scales over which a cooling age gradient may be resolved. The data presented here have the advantage of being from nearly 200 km to the east of previously reported sample sites. This large spacing should be optimal for resolving any west-east age gradients such that our data are important for ongoing evaluation of this model. The youngest reported AFT ages in the western Piedmont of North Carolina–Virginia range from ca. 127 to 111 Ma (Fig. 1; Spotila et al., 2004). This range is younger than the AFT ages of samples CG18-2 (133 Ma), CG18-4 (155 Ma), and CG18-8 (126 Ma), all in Virginia or North Carolina, but older than that of sample CG18-6 (99 Ma, in North Carolina). Thus, three out of four samples that lie within the area previously proposed and analyzed for escarpment retreat are consistent with the predictions of the escarpment-retreat model. However, thermochronologic analysis of additional plutons across a range of closure temperatures would help to better resolve this issue.

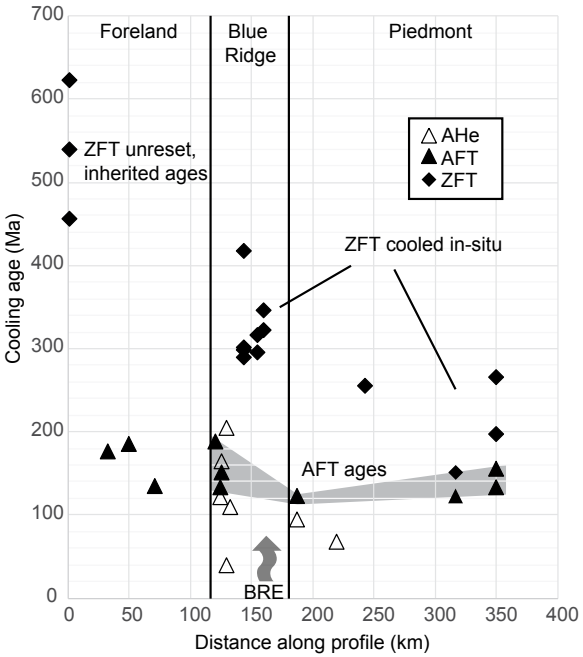

Figure 12. Zircon fission-track (ZFT), apatite fission-track (AFT), and apatite (U-Th)/He (AHe) ages along a transect extending from west (on left) to east (on right) across the Appalachian orogen of North Carolina. Transect location is shown on Figure 1. BRE—Blue Ridge escarpment.

It is also interesting to note that regionally, the oldest AFT ages in the Piedmont date to the Jurassic, with the modal age being Early Cretaceous (ca. 130 Ma; see Fig. 1 inset). The timing of this cooling lags by nearly 100 m.y. the timing of extensional deformation in the region. Thus, it seems likely that the ZFT and AFT systems resolve exhumational cooling related to the rejuvenation of rift-related topography by surface uplift after the Triassic. This rejuvenation may have been caused by magmatic heating of the crust in the Jurassic and possibly the Early Cretaceous (Fig. 11) or by other processes that modified the buoyancy of the lithosphere.

Lastly, our data may add to growing evidence for later rejuvenations of topography and exhumation in the southern Appalachians. For one, central North Carolina–South Carolina sites (samples CG18-6, Tar River; CG19-1, Congaree River; and, to a degree, CG18-12, Savannah River) exhibit slightly later cooling through the AFT closure temperature than sites to the north. Moreover, recently reported evidence for a Neogene rejuvenation includes short apatite fission tracks in the foreland basin province in southeastern Kentucky (e.g., Boettcher and Milliken, 1994), an increase in sediment flux to the eastern Gulf Coast (e.g., Combellas-Bigott and Galloway, 2006), and an acceleration in river incision in catchments located on the western side of the continental divide in western North Carolina (e.g., Gallen et al., 2013). Site CG18-6 (Tar River, North Carolina) exhibits a Neogene acceleration in exhumational cooling in the inverse modeling. The model result is driven by both the AFT age dispersion and the short track lengths in the sample. The sample site in our study is at a similar latitude to those of the other studies, but it is offset by hundreds of kilometers to the east. Thus, one promising avenue for future work may be to more fully evaluate the eastern extent of enhanced Cretaceous and/or Neogene erosion in the North Carolina–South Carolina portion of the Appalachians. Notably, our own analysis of coastal-plain stratigraphy indicates a regional transition from carbonate deposition in the middle Cenozoic to sand deposition in the later Cenozoic in downdip stratigraphic sections, and further underscores the need for additional investigation (Fig. 11; Brown et al., 1972; Scholle, 1979).

CONCLUSIONS

We have presented new ZFT and AFT cooling ages for six bedrock samples along the Fall Line from the James River in Virginia to the Savannah River on the border of Georgia and South Carolina, spanning a distance of 200 km. These fission-track data are paired with ZUPb and AUPb data. The ZUPb data are mostly consistent with previous mapping and geochronology, but the AUPb data at our northernmost and southernmost sample sites seem to resolve very rapid Pennsylvanian–Permian cooling of Carboniferous plutons shortly after emplacement. Although the ZFT age distributions are complex, they appear to resolve in situ cooling through ZFT closure temperatures (~282 °C) in the Jurassic across the region. AFT age distributions are less complex and resolve cooling through the AFT closure temperature (~116 °C) generally in the Late Jurassic–Early Cretaceous.

Inverse and forward modeling scenarios are used to evaluate the thermal history recorded by these samples. The models are partially constrained by the data described above and partially constrained by regional observations of thermal maturity and geologic relationships. They indicate that the post-Paleozoic thermal history for the Appalachian hinterland involves rapid exhumational cooling (>10 °C/m.y.) to near-surface temperatures by the Triassic, modest reburial in the Triassic (maximum burial heating on the order of 180 °C plus or minus tens of degrees), exhumational cooling in the Jurassic to Early Cretaceous (at rates of 1–10 °C/m.y.), and then slower exhumational cooling (~1 °C/m.y.) since that time. The inverse models resolve cooling through the AFT closure temperature in the Jurassic in central Virginia and North Carolina and slightly later in the Early Cretaceous in central North Carolina and South Carolina, similar to the spatial gradient in the measured AFT ages. Inverse modeling of one sample in the eastern Piedmont of central North Carolina suggests a possibility of a Neogene acceleration in cooling. The Triassic–Cretaceous heating and cooling likely reflects burial by Triassic strata and basin inversion, although the addition and dissipation of magmatic heat may be superimposed on this history. The later accelerations in cooling rates should be further investigated by follow-up studies. However, overall, the geological interpretations that derive from the space-time patterns of Cretaceous–Cenozoic cooling described above are supported by grain-size trends in offshore stratigraphic sections.

The regional patterns of cooling ages are consistent with the view that the macrogeomorphic evolution of the southern Appalachians was dominated by the erosional retreat of an escarpment. As opposed to being directly related to the timing of rifting, our modeling suggests that topography was rejuvenated in the Jurassic (and possibly in subsequent episodes) and that the rejuvenation was possibly related to regionally extensive magmatism.

ACKNOWLEDGMENTS

An early version of this manuscript benefitted from comments from Richard Lease. Suggestions from U.S. Geological Survey (USGS) peer reviewer Rebecca Stokes, *Geosphere* reviewer Jaclyn Baughman, an anonymous *Geosphere* reviewer, and Associate Editor G. Lang Farmer greatly improved this manuscript. This manuscript benefitted from petrographic reports by Spectrum Petrographics (Vancouver, Washington). This work was funded by the USGS Energy Resources Program. Any use of trade, firm, or product names is for descriptive purposes only and does not imply endorsement by the U.S. Government.

REFERENCES CITED

Almy, C.C., Jr., 1987, Lithostratigraphic-seismic evaluation of hydrocarbon potential, North Carolina coastal and continental margins: Interim report, year 2: Minerals Management Service and Association of American State Geologists: Raleigh, North Carolina, 18 p. with plates.

Applegate, A.V., Winston, G.O., and Palacas, J.G., 1981, Subdivision and regional stratigraphy of the pre–Punta Gorda rocks (lowermost Cretaceous–Jurassic?) in South Florida: Gulf Coast Association of Geological Societies Transactions, v. 31, p. 447–453.

Basler, L.C., Baughman, J.S., Fame, M.L., and Haproff, P.J., 2021, Spatially variable syn- and post-Alleghanian exhumation of the central Appalachian Mountains from zircon (U-Th)/He thermochronology: Geosphere, v. 17, p. 1151–1169, https://doi.org/10.1130/GES02368.1.

Blackmer, G.G., Omar, G.I., and Gold, D.P., 1994, Post-Alleghanian unroofing history of the Appalachian Basin, Pennsylvania, from apatite fission track analysis and thermal models: Tectonics, v. 13, p. 1259–1276, https://doi.org/10.1029/94TC01507.

Boettcher, S.S., and Milliken, K.L., 1994, Mesozoic-Cenozoic unroofing of the southern Appalachian Basin: Apatite fission track evidence from Middle Pennsylvanian sandstones:

The Journal of Geology, v. 102, p. 655–668, https://doi.org/10.1086/629710.

Brown, P.M., Miller, J.A., and Swain, F.M., 1972, Structural and stratigraphic framework and spatial distribution of permeability of the Atlantic Coastal Plain, North Carolina to New York: U.S. Geological Survey Professional Paper 796, 79 p., https://doi.org/10.3133/pp796.

Burtner, R.L., Nigrini, A., and Donelick, R.A., 1994, Thermochronology of Lower Cretaceous source rocks in the Idaho-Wyoming thrust belt: American Association of Petroleum Geologists Bulletin, v. 78, p. 1613–1636, https://doi.org/10.1306/A25FF233-171B-11D7-8645000102C1865D.

Chew, D.M., and Donelick, R.A., 2012, Combined apatite fission track and U-Pb dating by LA-ICP-MS and its application in apatite provenance analysis, *in* Sylvester, P., ed., Quantitative Mineralogy and Microanalysis of Sediments and Sedimentary Rocks: Mineralogical Association of Canada Short Course 42, p. 219–247.

Cochrane, R., Spikings, R.A., Chew, D.M., Wotzlaw, J.-F., Chiaradia, M., Tyrrell, S., Schaltegger, U., and Van der Lelij, R., 2014, High temperature (>350 °C) thermochronology and mechanisms of Pb loss in apatite: Geochimica et Cosmochimica Acta, v. 127, p. 39–56, https://doi.org/10.1016/j.gca.2013.11.028.

Cogné, N., and Gallagher, K., 2021, Some comments on the effect of uranium zonation on fission track dating by LA-ICP-MS: Chemical Geology, v. 573, https://doi.org/10.1016/j.chemgeo.2021.120226.

Combellas-Bigott, R.I., and Galloway, W.E., 2006, Depositional and structural evolution of the middle Miocene depositional episode, east-central Gulf of Mexico: American Association of Petroleum Geologists Bulletin, v. 90, p. 335–362, https://doi.org/10.1306/10040504132.

Craddock, W.H., and O'Sullivan, P.B., 2021, Apatite and zircon U/Pb and fission track geo- and thermo-chronologic data along the Fall Line of the southeastern United States: U.S. Geological Survey Data Release, https://doi.org/10.5066/P9UAWI41.

Dallmeyer, R.D., Wright, J.E., Secor, D.T., Jr., and Snoke, A.W., 1986, Character of the Alleghanian orogeny in the southern Appalachians: Part II. Geochronological constraints on the tectonothermal evolution of the eastern Piedmont in South Carolina: Geological Society of America Bulletin, v. 97, p. 1329–1344, https://doi.org/10.1130/0016-7606(1986)97<1329:COTAOI>2.0.CO;2.

Dickinson, W.R., and Gehrels, G.E., 2009, Use of U-Pb ages of detrital zircons to infer maximum depositional ages of strata: A test against a Colorado Plateau Mesozoic database: Earth and Planetary Science Letters, v. 288, p. 115–125, https://doi.org/10.1016/j.epsl.2009.09.013.

Dillon, W.P., and Popenoe, P., 1988, The Blake Plateau Basin and Carolina Trough, *in* Sheridan, R.E., and Grow, J.A., eds., The Atlantic Continental Margin: Boulder, Colorado, Geological Society of America, The Geology of North America, v. I-2, p. 291–328, https://doi.org/10.1130/DNAG-GNA-I2.291.

Donelick, R.A., O'Sullivan, P.B., and Ketcham, R.A., 2005, Apatite fission-track analysis: Reviews in Mineralogy and Geochemistry, v. 58, p. 49–94, https://doi.org/10.2138/rmg.2005.58.3.

Durrant, J.M., 1979, Structural and metamorphic history of the Virginia Piedmont province near Richmond, Virginia [M.S. thesis]: Columbus, Ohio State University, 117 p.

Fullagar, P.D., and Butler, J.R., 1979, 325 to 265 m.y.-old granitic plutons in the Piedmont of the southeastern Appalachians: American Journal of Science, v. 279, p. 161–185, https://doi.org/10.2475/ajs.279.2.161.

Galbraith, R.F., 1981, On statistical models for fission track counts: Journal of the International Association for Mathematical Geology, v. 13, p. 471–478, https://doi.org/10.1007/BF01034498.

Galbraith, R.F., 1988, Graphical display of estimates having different standard error: Technometrics, v. 30, p. 271–281, https://doi.org/10.1080/00401706.1988.10488400.

Galbraith, R.F., 1990, The radial plot: Graphical assessment of spread in ages: Nuclear Tracks and Radiation Measurements, v. 17, p. 207–214, https://doi.org/10.1016/1359-0189(90)90036-W.

Galbraith, R.F., 2005, Statistics for Fission Track Analysis: Boca Raton, Florida, Chapman and Hall/CRC Press, 219 p., https://doi.org/10.1201/9781420034929.

Gallen, S.F., Wegmann, K.W., and Bohnenstiehl, D.R., 2013, Miocene rejuvenation of topographic relief in the southern Appalachians: GSA Today, v. 23, no. 2, p. 4–10, https://doi.org/10.1130/GSATG163A.1.

Ganerød, M., Chew, D.M., Smethurst, M.A., Troll, V.R., Corfu, F., Meade, F., and Prestvik, T., 2011, Geochronology of the Tardree Rhyolite Complex, Northern Ireland: Implications for zircon fission track studies, the North Atlantic Igneous Province and the age of the Fish Canyon sanidine standard: Chemical Geology, v. 286, p. 222–228, https://doi.org/10.1016/j.chemgeo.2011.05.007.

Gates, A.E., and Glover, L., III, 1989, Alleghanian tectono-thermal evolution of the dextral transcurrent Hylas zone, Virginia Piedmont, U.S.A.: Journal of Structural Geology, v. 11, p. 407–419, https://doi.org/10.1016/0191-8141(89)90018-7.

Gay, N.K., 2004, The bedrock geology of the western portion of the Rocky Mount 100k quadrangle, Nash, Wilson, and Edgecombe counties, North Carolina: North Carolina Geological Survey Open-File Report 2004-05, North Carolina Department of Environmental Quality, Raleigh, North Carolina, 1 sheet, scale 1:100,000.

Hames, W.E., Renne, P.R., and Ruppel, C., 2000, New evidence for geologically instantaneous emplacement of earliest Jurassic Central Atlantic magmatic province basalts on the North American margin: Geology, v. 28, p. 859–862, https://doi.org/10.1130/0091-7613(2000)28<859:NEFGIE>2.0.CO;2.

Hasebe, N., Barbarand, J., Jarvis, K., Carter, A., and Hurford, A.J., 2004, Apatite fission-track chronometry using laser ablation ICP-MS: Chemical Geology, v. 207, p. 135–145, https://doi.org/10.1016/j.chemgeo.2004.01.007.

Hasebe, N., Tamura, A., and Arai, S., 2013, Zeta equivalent fission-track dating using LA-ICP-MS and examples with simultaneous U-Pb dating: Island Arc, v. 22, p. 280–291, https://doi.org/10.1111/iar.12040.

Hatcher, R.D., 1987, Tectonics of the southern and central Appalachian internides: Annual Review of Earth and Planetary Sciences, v. 15, p. 337–362, https://doi.org/10.1146/annurev.ea.15.050187.002005.

Heffner, D.M., Knapp, J.H., Akintunde, O.M., and Knapp, C.C., 2012, Preserved extent of Jurassic flood basalt in the South Georgia Rift: A new interpretation of the J horizon: Geology, v. 40, p. 167–170, https://doi.org/10.1130/G32638.1.

Hibbard, J.P., Stoddard, E.F., Secor, D.T., and Dennis, A.J., 2002, The Carolina Zone: Overview of Neoproterozoic to Early Paleozoic peri-Gondwanan terranes along the eastern flank of the southern Appalachians: Earth-Science Reviews, v. 57, p. 299–339, https://doi.org/10.1016/S0012-8252(01)00079-4.

Horton, J.W., Jr., and Dicken, C.L., 2001, Preliminary digital geologic map of the Appalachian Piedmont and Blue Ridge, South Carolina segment: U.S. Geological Survey Open-File Report 2001–298, https://doi.org/10.3133/ofr01298.

Ketcham, R.A., 2005, Forward and inverse modeling of low-temperature thermochronometry data: Reviews in Mineralogy and Geochemistry, v. 58, p. 275–314, https://doi.org/10.2138/rmg.2005.58.11.

Ketcham, R.A., 2016, HeFTy version 1.9.1: Austin, Texas, 85 p.

Ketcham, R.A., Carter, A., Donelick, R.A., Barbarand, J., and Hurford, A.J., 2007, Improved modeling of fission-track annealing in apatite: American Mineralogist, v. 92, p. 799–810, https://doi.org/10.2138/am.2007.2281.

Kohn, B.P., Wagner, M.E., Lutz, T.M., and Organist, G., 1993, Anomalous Mesozoic thermal regime, central Appalachian Piedmont: Evidence from sphene and zircon fission-track dating: The Journal of Geology, v. 101, p. 779–794, https://doi.org/10.1086/648274.

Kunk, M.J., Wintsch, R.P., Naeser, C.W., Naeser, N.D., Southworth, C.S., Drake, A.A., Jr., and Becker, J.L., 2005, Contrasting tectonothermal domains and faulting in the Potomac terrane, Virginia-Maryland—Discrimination by $^{40}Ar/^{39}Ar$ and fission-track thermochronology: Geological Society of America Bulletin, v. 117, p. 1347–1366, https://doi.org/10.1130/B25599.1.

Lanphere, M.A., 1983, $^{40}Ar/^{39}Ar$ ages of basalt from Clubhouse Crossroads test hole #2, near Charleston South Carolina, *in* Gohn, G.S., ed., Studies Related to the Charleston, South Carolina, Earthquake of 1886—Tectonics and Seismicity: U.S. Geological Survey Professional Paper 1313, p. B1–B8.

Lawton, D.E., Moye, F.J., Murray, J.B., O'Connor, B.J., Penley, H.M., Sandrock, G.S., Marsalis, W.E., Friddell, M.S., Hetrick, J.H., Huddlestun, P.F., Hunter, R.E., Mann, W.R., Martin, B.F., Pickering, S.M., Schneeberger, F.J., and Wilson, J.D., 1976, Geologic map of Georgia: Atlanta, Environmental Protection Division, Georgia Department of Natural Resources, scale 1:500,000.

Ludwig, K.R., 2012, User's manual for Isoplot version 3.75–4.15: A geochronological toolkit for Microsoft Excel: Berkeley Geochronological Center Special Publication 5, 75 p.

Malinconico, M.L., 2015, Triassic Taylorsville basin, Virginia, USA: Comparative thermal history and organic facies within the early Mesozoic eastern North American lacustrine rift basin system, *in* Post, P.J., Coleman, J.L., Jr, Rosen, N.C., Brown, D.E., Roberts-Ashby, T., Kahn, P., and Rowan, M., eds., Petroleum Systems in "Rift" Basins: 34th Annual GCSSEPM Foundation Perkins-Rosen Research Conference, December 13–16, 2015, Houston, Texas: SEPM (Society for Sedimentary Geology) GCSSEPM 34, p. 215–251, https://doi.org/10.5724/gcs.15.34.0215.

Marr, J.D., Jr., 2002, Geologic map of the western portion of the Richmond 30 × 60 minute quadrangle, Virginia: Virginia Division of Mineral Resources Publication 165, scale 1:100,000.

Mazza, S.E., Gazel, E., Johnson, E.A., Bizimis, M., McAleer, R., and Biryol, C.B., 2017, Post-rift magmatic evolution of the eastern North American "passive-aggressive" margin: Geochemistry Geophysics Geosystems, v. 18, p. 3–22, https://doi.org/10.1002/2016GC006646.

McBride, J.H., Nelson, K.D., and Brown, L.D., 1989, Evidence and implications of an extensive Mesozoic rift basin and basalt/diabase sequence beneath the southeast Coastal Plain: Geological Society of America Bulletin, v. 101, p. 512–520, https://doi.org/10.1130/0016-7606(1989)101<0512:EAIOAE>2.3.CO;2.

McDannell, K.T., Issler, D.R., and O'Sullivan, P.B., 2019, Radiation-enhanced fission track annealing revisited and consequences for apatite thermochronometry: Geochimica et Cosmochimica Acta, v. 252, p. 213–239, https://doi.org/10.1016/j.gca.2019.03.006.

McKeon, R.E., Zeitler, P.K., Pazzaglia, F.J., Idleman, B.D., and Enkelmann, E., 2014, Decay of an old orogen: Inferences about Appalachian landscape evolution from low-temperature thermochronology: Geological Society of America Bulletin, v. 126, p. 31–46, https://doi.org/10.1130/B30808.1.

Mueller, P., Heatherington, A., Foster, D., and Wooden, J., 2011, Alleghanian granites of the southern Appalachian orogen: Keys to Pangean reconstructions, *in* Huebner, M.T., and Hatcher, R.D., Jr., eds., The Geology of the Inner Piedmont at the Northeast End of the Pine Mountain Window: Georgia Geological Society Guidebook 31, p. 39–48.

Müller, R.D., Sdrolias, M., Gaina, C., and Roest, W.R., 2008, Age, spreading rates, and spreading symmetry of the world's ocean crust: Geochemistry Geophysics Geosystems, v. 9, Q04006, https://doi.org/10.1029/2007GC001743.

Naeser, C.W., Naeser, N.D., Newell, W.L., Southworth, S., Edwards, L.E., and Weems, R.E., 2016, Erosional and depositional history of the Atlantic passive margin as recorded in detrital zircon fission-track ages and lithic detritus in Atlantic coastal plain sediments: American Journal of Science, v. 316, p. 110–168, https://doi.org/10.2475/02.2016.02.

North Carolina Geological Survey, 1985, Geologic map of North Carolina: Raleigh, North Carolina Department of Natural Resources and Community Development, Geological Survey Section, scale 1:500,000.

Olsen, P.E., 1997, Stratigraphic record of the early Mesozoic breakup of Pangea in the Laurasia-Gondwana rift system: Annual Review of Earth and Planetary Sciences, v. 25, p. 337–401, https://doi.org/10.1146/annurev.earth.25.1.337.

Olsen, P.E., Kent, D.V., Et-Touhami, M., and Puffer, J., 2003, Cyclo-, magneto-, and bio-stratigraphic constraints on the duration of the CAMP event and its relationship to the Triassic-Jurassic boundary, *in* Hames, W., McHone, J.G., Renne, P., and Ruppel, C., eds., The Central Atlantic Magmatic Province: Insights from Fragments of Pangea: American Geophysical Union Geophysical Monograph 136, p. 7–32, https://doi.org/10.1029/136GM02.

Owens, B.E., Carter, M., and Bailey, C.M., 2017, Geology of the Petersburg batholith, eastern Piedmont, Virginia, *in* Bailey, C.M., and Jaye, S., eds., From the Blue Ridge to the Beach: Geological Field Excursions across Virginia: Geological Society of America Field Guide 47, p. 153–162, https://doi.org/10.1130/2017.0047(06).

Owens, J.P., and Gohn, G.S., 1985, Depositional history of the Cretaceous Series in the U.S. Atlantic Coastal Plain: Stratigraphy, paleoenvironments, and tectonic controls of sedimentation, *in* Poag, C.W., ed., Geologic Evolution of the United States Atlantic Margin: New York, Van Nostrand Reinhold, p. 25–86.

Paces, J.B., and Miller, J.D., Jr., 1993, Precise U-Pb ages of Duluth Complex mafic intrusions, northeastern Minnesota: Geochronological insights to physical, petrogenetic, paleomagnetic, and tectonomagmatic processes associated with the 1.1 Ga Midcontinent Rift System: Journal of Geophysical Research, v. 98, p. 13,997–14,013, https://doi.org/10.1029/93JB01159.

Pazzaglia, F.J., and Brandon, M.T., 1996, Macrogeomorphic evolution of the post-Triassic Appalachian mountains determined by deconvolution of the offshore basin sedimentary record: Basin Research, v. 8, p. 255–278, https://doi.org/10.1046/j.1365-2117.1996.00274.x.

Poag, C.W., and Sevon, W.D., 1989, A record of Appalachian denudation in postrift Mesozoic and Cenozoic sedimentary deposits of the U.S. Middle Atlantic continental margin: Geomorphology, v. 2, p. 119–157, https://doi.org/10.1016/0169-555X(89)90009-3.

Post, P.J., Klazynski, R.J., Klocek, E.S., Riches, T.J., Jr., and Li, K., 2016, Inventory of technically and economically recoverable hydrocarbon resources of the Atlantic Outer Continental Shelf as of January 1, 2014: U.S. Bureau of Ocean Energy Management OCS Report 2016-071, 62 p.

Rahn, M.K., Brandon, M.T., Batt, G.E., and Garver, J.I., 2004, A zero-damage model for fission-track annealing in zircon: American Mineralogist, v. 89, p. 473–484, https://doi.org/10.2138/am-2004-0401.

Reed, J.S., Spotila, J.A., Eriksson, K.A., and Bodnar, R.J., 2005, Burial and exhumation history of Pennsylvanian strata, central Appalachian basin: An integrated study: Basin Research, v. 17, p. 259–268, https://doi.org/10.1111/j.1365-2117.2005.00265.x.

Reid, J.C., and Milici, R.C., 2008, Hydrocarbon source rocks in the Deep River and Dan River Triassic basins, North Carolina: U.S. Geological Survey Open-File Report 2008-1108, 28 p., https://doi.org/10.3133/ofr20081108.

Reiners, P.W., and Brandon, M.T., 2006, Using thermochronology to understand orogenic erosion: Annual Review of Earth and Planetary Sciences, v. 34, p. 419–466, https://doi.org/10.1146/annurev.earth.34.031405.125202.

Roden, M.K., 1991, Apatite fission-track thermochronology of the southern Appalachian Basin: Maryland, West Virginia, and Virginia: The Journal of Geology, v. 99, p. 41–53, https://doi.org/10.1086/629472.

Roden, M.K., and Miller, D.S., 1989, Apatite fission-track thermochronology of the Pennsylvania Appalachian Basin: Geomorphology, v. 2, p. 39–51, https://doi.org/10.1016/0169-555X(89)90005-6.

Roden, M.K., and Miller, D.S., 1991, Tectono-thermal history of Hartford, Deerfield, Newark and Taylorsville Basins, eastern United States, using fission-track-analysis: Schweizerische Mineralogische und Petrographische Mitteilungen, v. 71, p. 187–203, https://doi.org/10.5169/seals-54356.

Roden, M.K., Elliot, W.C., Aronson, J.T., and Miller, D.S., 1993, A comparison of fission-track ages of apatite and zircon to the K/Ar ages of illite-smectite (I/S) from Ordovician K-bentonites of southern Appalachian basin: The Journal of Geology, v. 101, p. 633–641, https://doi.org/10.1086/648254.

Samson, S.D., Coler, D.G., and Sper, J.A., 1995, Geochemical and Nd-Sr-Pb isotopic composition of the Alleghanian granites of the southern Appalachians: Origin, tectonic setting, and source characterization: Earth and Planetary Science Letters, v. 134, p. 359–376, https://doi.org/10.1016/0012-821X(95)00124-U.

Schlische, R.W., 2003, Progress in understanding the structural geology, basin evolution, and tectonic history of the eastern North American rift system, *in* LeTourneau, P.M., and Olsen, P.E., eds., The Great Rift Valleys of Pangea in Eastern North America—Volume One: Tectonics, Structure, and Volcanism: New York, Columbia University Press, p. 21–64, https://doi.org/10.7312/leto11162-003.

Schoene, B., and Bowring, S.A., 2006, U-Pb systematics of the McClure Mountain syenite: Thermochronological constraints on the age of the $^{40}Ar/^{39}Ar$ standard MMhb: Contributions to Mineralogy and Petrology, v. 151, p. 615–630, https://doi.org/10.1007/s00410-006-0077-4.

Scholle, P.A., ed., 1979, Geological Studies of the COST GE-1 well, United States South Atlantic outer continental shelf area: U.S. Geological Survey Circular 800, 114 p., https://doi.org/10.3133/cir800.

Spotila, J.A., Bank, G.C., Reiners, P.W., Naeser, C.W., Naeser, N.D., and Henika, B.S., 2004, Origin of the Blue Ridge escarpment along the passive margin of eastern North America: Basin Research, v. 16, p. 41–63, https://doi.org/10.1111/j.1365-2117.2003.00219.x.

Stacey, J.S., and Kramers, J.D., 1975, Approximation of terrestrial lead isotope evolution by a two-stage model: Earth and Planetary Science Letters, v. 26, p. 207–221, https://doi.org/10.1016/0012-821X(75)90088-6.

Sweeney, J.J., and Burnham, A.K., 1990, Evaluation of a simple model of vitrinite reflectance based on chemical kinetics: American Association of Petroleum Geologists Bulletin, v. 74, p. 1559–1570, https://doi.org/10.1306/0C9B251F-1710-11D7-8645000102C1865D.

Tseng, H.-Y., Onstott, T.C., Burruss, R.C., and Miller, D.S., 1996, Constraints on the thermal history of Taylorsville Basin, Virginia, U.S.A., from fluid-inclusion and fission-track analyses: Implications for subsurface geomicrobiology experiments: Chemical Geology, v. 127, p. 297–311, https://doi.org/10.1016/0009-2541(95)00130-1.

Vermeesch, P., 2009, RadialPlotter: A Java application for fission track, luminescence, and other radial plots: Radiation Measurements, v. 44, p. 409–410, https://doi.org/10.1016/j.radmeas.2009.05.003.

Vermeesch, P., 2017, Statistics for LA-ICP-MS based fission track dating: Chemical Geology, v. 456, p. 19–27, https://doi.org/10.1016/j.chemgeo.2017.03.002.

Vermeesch, P., 2018, IsoplotR: A free and open toolbox for geochronology: Geoscience Frontiers, v. 9, p. 1479–1493, https://doi.org/10.1016/j.gsf.2018.04.001.

Weems, R.E., Lewis, W.C., and Aleman-Gonzalez, W.B., 2009, Surficial geologic map of the Roanoke Rapids 30′ × 60′ quadrangle, North Carolina: U.S. Geological Survey Open-File Report 2009-1149, scale 1:100,000, https://doi.org/10.3133/ofr20091149.

Withjack, M.O., Schlische, R.W., and Olsen, P.E., 1998, Diachronous rifting, drifting, and inversion on the passive margin of central eastern North America: An analog for other passive margins: American Association of Petroleum Geologists Bulletin, v. 82, p. 817–835.

Yamada, R., Murakami, M., and Tagami, T., 2007, Statistical modelling of annealing kinetics of fission tracks in zircon: Reassessment of laboratory experiments: Chemical Geology, v. 236, p. 75–91, https://doi.org/10.1016/j.chemgeo.2006.09.002.